Science of the Total Environment 878 (2023) 163124

Contents lists available at ScienceDirect

Science of the Total Environment

journal homepage: www.elsevier.com/locate/scitotenv

Unveiling resilience mechanisms of *Quercus ilex* seedlings to severe water stress: Changes in non-structural carbohydrates, xylem hydraulic functionality and wood anatomy

Antonella Gori [a,b,*], Barbara Baesso Moura [a], Fabiano Sillo [b], Francesca Alderotti [a], Dalila Pasquini [a], Raffaella Balestrini [b], Francesco Ferrini [a,b], Mauro Centritto [b], Cecilia Brunetti [b,*]

[a] University of Florence, Department of Agriculture, Food, Environment and Forestry (DAGRI), Sesto Fiorentino, Florence 50019, Italy
[b] National Research Council of Italy, Institute for Sustainable Plant Protection (IPSP), Sesto Fiorentino, Florence and Turin 50019 and 10135, Italy

HIGHLIGHTS

- Water stress and recovery impacted holm oak seedlings wood parenchyma.
- *Q. ilex* reduced xylem functionality and NSCs content in wood parenchyma.
- Genes related to sugar mobilization and cell wall remodeling were upregulated.
- The strong reduction in g_s did not prevent xylem embolism under water stress.
- NSCs were completely restore after thirty days of rewatering.

GRAPHICAL ABSTRACT

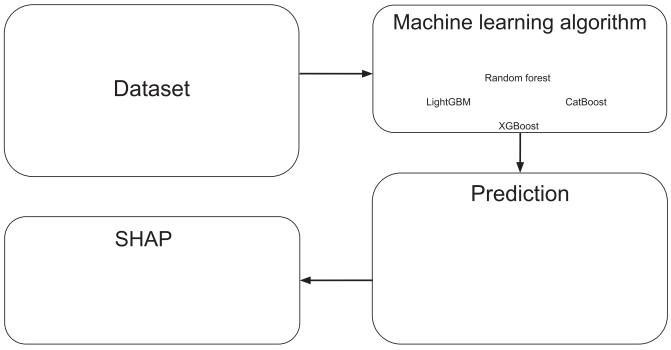

ARTICLE INFO

Editor: Zhaozhong Feng

Keywords:
Quercus ilex
Non-structural carbohydrates (NSCs)
Drought responsive genes
Xylem embolism
Water stress
Rewatering
Wood parenchyma

ABSTRACT

Over the last few decades, extensive dieback and mortality episodes of *Quercus ilex* L. have been documented after severe drought events in many Mediterranean forests. However, the underlying physiological, anatomical, and biochemical mechanisms remain poorly understood. We investigated the physiological and biochemical processes linked to embolism formation and non-structural carbohydrates (NSCs) dynamics in *Q. ilex* seedlings exposed to severe water stress and rewatering. Measurements of leaf gas exchange, water relations, non-structural carbohydrates, drought-related gene expression, and anatomical changes in wood parenchyma were assessed. Under water stress, the midday stem water potential dropped below - 4.5 MPa corresponding to a ~ 50 % loss of hydraulic conductivity. A 70 % reduction in stomatal conductance led to a strong depletion of wood NSCs. Starch consumption, resulting from the up-regulation of the β-amylase gene *BAM3*, together with the downregulation of glucose (*GPT1*) and sucrose (*SUC27*) transport genes, suggests glucose utilization to sustain cellular metabolism in the wood parenchyma. After rewatering, the presence of residual xylem embolism led to an incomplete recovery of leaf gas exchanges. However, the partial restoration of photosynthesis allowed the accumulation of new starch reserves in the wood parenchyma and the production of new narrower vessels. In addition, changes in the cell wall composition of the wood parenchyma fibers were observed. Our findings indicate that thirty days of rewatering were sufficient to restore the NSCs reserves and growth rates of *Q. ilex* seedlings and that the carryover effects of water stress were primarily caused by hydraulic dysfunction.

* Correspondance to: C. Brunetti, National Research Council of Italy, Institute for Sustainable Plant Protection (IPSP), 50019 Sesto Fiorentino, Florence, Italy; A. Gori, University of Florence, Department of Agriculture, Food, Environment and Forestry (DAGRI), 50019 Sesto Fiorentino, Florence, Italy.
E-mail addresses: antonella.gori@unifi.it (A. Gori), cecilia.brunetti@ipsp.cnr.it (C. Brunetti).

http://dx.doi.org/10.1016/j.scitotenv.2023.163124
Received 27 December 2022; Received in revised form 21 March 2023; Accepted 23 March 2023
Available online 30 March 2023

1. Introduction

Severe drought events have led to a rapid increase in tree mortality in many ecosystems worldwide (Anderegg et al., 2020; Anderegg et al., 2018; Allen et al., 2010; Brodribb et al., 2020). In the Western Mediterranean area, dieback phenomena have been observed in different oak species after anomalous drought and heat waves (Galiano et al., 2012; Gentilesca et al., 2017). The holm oak (*Quercus ilex* L., Fagaceae) is an evergreen sclerophyll tree or shrub that dominates the landscape of several Mediterranean coastal and sub-coastal areas, and is widely used in artificial reforestation programs (González-Rodríguez et al., 2011). Thus, holm oak is a keystone species for the ecosystem services of Mediterranean basin forests, which have been recognized as biodiversity hotspots in terms of number of species and endemism (Mittermeier et al., 2011). Besides its ecological importance, this species also possesses a great economic value, being the most representative tree of the agrosilvopastoral systems of *dehesa*, covering almost four million hectares in the Iberian Península (Joffre et al., 1999).

Nowadays, Mediterranean holm oak forests are facing severe problems and challenges. Indeed, extensive holm oak diebacks have been recently observed following severe drought episodes (Colangelo et al., 2018; Encinas-Valero et al., 2021; Ogaya et al., 2015, 2020; Pasquini et al., 2023). Therefore, improving our understanding of the mechanisms underlying holm oak decline and mortality is required to predict *Q. ilex* forest loss and suggest management measures for its conservation (Gentilesca et al., 2017; McDowell et al., 2022). Previous studies have shown that *Q. ilex* displays an isohydric behaviour under water stress because it tightly controls stomatal conductance, thus preventing leaf dehydration and embolism formation in xylem vessels (David et al., 2007; Limousin et al., 2022; Nardini et al., 2014; Vaz et al., 2010). Indeed, in this species, stomatal closure occurs at water potentials much higher than those inducing a 50 % loss of hydraulic conductivity (Peguero-Pina et al., 2014; Vilagrosa et al., 2003). Nevertheless, it has been demonstrated that under prolonged water stress, despite an almost complete stomatal closure, *Q. ilex* seedlings are still exposed to significant losses in hydraulic conductivity (Peguero-Pina et al., 2018).

Recently, renewed attention has been given to xylem-associated parenchyma because of its key role in regulating xylem hydraulics (Kiorapostolou et al., 2019). This tissue, formed by vessel-associated cells and rays, is of primary importance for plant mechanical support, water storage and movement (Holbrook, 2002; Pfautsch et al., 2015). For example, it has been demonstrated that aquaporin genes located in the wood parenchyma cells surrounding xylem vessels are overexpressed in response to drought and have a crucial role in hydraulic recovery (Chitarra et al., 2014; Pfautsch et al., 2015; Secchi et al., 2017; Steppe et al., 2012). These transmembrane water and solute transporter channels are involved in water flow from living stem cells to xylem conduits, thereby regulating stem radial hydraulic conductance (Feltrim et al., 2021; Shatil-Cohen et al., 2011). In addition, wood parenchyma cells surrounding vessels are involved in the loading/unloading of solutes into/from the transpiration stream and the storage and mobilization of non-structural carbohydrates (NSCs) (Słupianek et al., 2021; Zwieniecki and Holbrook, 2009). It has been reported that, in *Q. ilex*, starch reserves are reduced to release soluble sugars in response to water stress (Rodríguez-Calcerrada et al., 2017, 2021). Soluble sugars play a key role in osmotic potential adjustments and in preserving xylem functionality both under water stress and after re-watering (Brunetti et al., 2020; Secchi and Zwieniecki, 2016; Tomasella et al., 2019a). At the molecular level, NSCs mobilization derives from starch breakdown through the enzymes α and β amylases encoded by the BAM gene family (Zeeman et al., 2010), the expression of which is upregulated under carbon shortage conditions (Monroe and Storm, 2018; Thalmann and Santelia, 2017).

Previous studies have shown that changes in hydraulic conductance are often associated with changes in the anatomical characteristics of the wood (Corcuera et al., 2004; Poorter et al., 2010). These modifications are not only related to the number and diameter of xylem vessels (Camarero et al., 2016; Lens et al., 2022) but also to the expression of particular genes linked to lignification of the wood parenchyma and cell wall remodeling (Arend and Fromm, 2007; Mertz and Brutnell, 2014; Ohtsuka et al., 2018; Plavcová et al., 2013). However, additional research linking the anatomical, physiological, and molecular aspects of wood parenchyma may shed light on the changes in hydraulic traits and carbon metabolism *of Q. ilex* under water stress and rewatering.

The main objective of this study was to investigate the effect of water stress and rewatering on *Q. ilex* xylem functionality and NSCs levels in wood parenchyma. Because contrasting results have been reported in the literature regarding the drought responses of this species, gene expression analysis was applied to elucidate the molecular basis underlying wood anatomical, hydraulic, and carbon-related adjustments. Specifically, we expected that i) under water stress, the strict stomatal control of *Q. ilex* would avoid stem xylem hydraulic dysfunction and concomitantly lead to a reduction of NSCs in wood parenchyma cells; and ii) after rewatering, NSCs wood reserves would be restored due to the recovery of photosynthetic capacity.

2. Material and methods

2.1. Plant material and experimental design

Three-year-old *Quercus ilex* L. (holm oak) plants were purchased from a local nursery. Plants were transplanted in 6,5 L pots with a peat/pumice substrate (50:50, *v*/v) and grown in the greenhouse of the University of Florence, Italy (43°460 N, 11°150 E) for three months before starting the water stress imposition. Air temperature (°C) and relative humidity (RH, %) were measured at the tree height and recorded every 10 min (both parameters using sensors AM2315 of Adafruit Industries LLC, NY, USA). Plants were approximately 75–85 cm tall and 1 cm in diameter at the base when water stress imposition started. Twenty plants were equally spaced and randomly assigned to different experimental categories: well-watered (control plants for water stress (WW, five plants) and re-watering (R-WW, five plants), water-stressed (WS, five plants), and re-watered (R-WS, five plants) plants (Fig. SM1). Before assigning plants to each category, preliminary measurements of photosynthesis (P_n, μmol m^{-2} s^{-1}), stomatal conductance (g_s, mmol m^{-2} s^{-1}), maximum photochemical efficiency of photosystem II (F_v/fm), and leaf water potential (Ψ_{leaf}, MPa) were conducted to exclude significant differences among plants ($p > 0.05$).

At the beginning of the experiment (10th June 2019), WW and R-WW plants were irrigated daily to pot capacity, whereas a water stress treatment was applied to WS and R-WS plants, providing 70 % of the fraction of transpirable soil water (FTSW) (Brunetti et al., 2018). Water stress progression was monitored by measuring leaf gas exchanges every day, and after 30 days, when mean g_s values of stressed plants were roughly 30 % of controls, WW and WS plants were measured and sampled (10th July 2019). Then, R-WS and R-WW plants were irrigated to pot capacity (100 % FTSW) for 30 days before sampling (9th August 2019). The same experimental plan was repeated the following year (from the 10th of June 2020 to 10th August 2020), utilizing additional twenty-three-year-old holm oak plants (of the same size and bought from the same nursery) under the greenhouse conditions described above. The experimental plan and the list of measurements performed in the two years are shown in Fig. SM1.

2.2. Leaf physiological measurements

Photosynthesis (P_n, μmol m^{-2} s^{-1}), stomatal conductance (g_s, mmol m^{-2} s^{-1}), and photosystem II actual efficiency (Φ_{PSII}) were measured on five plants per treatment. Three fully expanded and healthy leaves per plant were measured and combined to make an individual replicate. Measurements were acquired using a portable infra-red gas analyzer (LI-6400, Li-Cor, Lincoln, NE, USA), with a cuvette of 2 cm^2 at a CO_2 concentration of 414 μmol mol^{-1}, a photosynthetic photon flux density of 1000 μmol m^{-2} s^{-1} and a leaf temperature of 25 °C. Then, the same leaves were dark-adapted for 30 min and used to measure the maximum photochemical efficiency of photosystem II (F_v/fm) using a portable chlorophyll fluorescence system (Handy Pea, Hansatech, Norflolk, United Kingdom).

Three leaves per plant were collected from five plants, wrapped in parafilm, and transported to the laboratory in a fridge bag to measure leaf fresh weight (FW). The leaves were then hydrated until saturation (constant weight) for 48 h in the dark to determine turgid weight (TW). The dry weight (DW) was obtained after drying the leaves at 80 °C for 48 h. Finally, the relative water content (RWC, %) was calculated using the following equation (Eq. (1)):

$$\mathrm{RWC}\ (\%) = (\mathrm{FW} - \mathrm{DW})/(\mathrm{TW} - \mathrm{DW}) \quad (1)$$

Leaf water potential (Ψ_{leaf}, MPa) was measured at pre-dawn (04:00–5:00 h) and midday (13:00–14:00 h) on two leaves per plant (combined to make an individual replicate) from five plants using a Scholander-type pressure chamber (PMS Instruments, Corvallis, OR, USA). The difference between midday (Ψ_{MD}, MPa) and pre-dawn water potentials (Ψ_{PD}, MPa) was calculated as $-\Delta\Psi = \Psi_{MD} - \Psi_{PD}$.

2.3. Hydraulic measurements

The xylem water potential (Ψ_{stem}, MPa) was measured by installing a stem psychrometer (PSY1; ICT International, Armidale, NSW, Australia) in the central region of the main stem of five plants per treatment (n = 5). After the instrument was clamped to the stem, the psychrometer was air-tight sealed with parafilm and silicone and then wrapped in foam rubber to ensure temperature stability. The Peltier cooling time was set from 10 s (for the WW and R-WW plants) to a maximum of 30 s (for the WS plants), and the interval time for data acquisition was set to 10 min. Moreover, Ψ_{stem} measured by a stem psychrometer was periodically validated with measurements conducted with a Scholander-type pressure chamber on leaves previously sealed with tin foil for one hour.

The percentage loss of xylem hydraulic conductivity (PLC, %) was assessed following the protocol described by Tomasella et al. (2019a). In detail, Ψ_{stem} was determined on bagged leaves and the main stem was cut 10 cm above the root collar underwater. Xylem tension was released by immersing the cut end in water and allowing the branch to rehydrate until Ψ_{stem} was higher than −0.5 MPa (Torres-Ruiz et al., 2015). Then, holding the entire branch underwater, a second cut was made approximately 75 cm from the initial cut (that is, higher than the maximum vessel length, as checked during preliminary analyses according to the methodology of Wang et al. (2014)). Hydraulic measurements were then conducted on a straight 7–12 cm long segment. Both ends of the stem segment were deprived of a portion of the bark (0.5 cm) and shaved underwater with a razor blade before being connected to a custom-made hydraulic apparatus. PLC was calculated as $\mathrm{PLC} = [1\text{-}(K_i / K_{max})] \times 100$, where K_i is the native stem hydraulic conductivity gravimetrically measured though a water head of 4 kPa, and K_{max} is the maximum hydraulic conductivity measured after embolism removal by flushing the sample at high pressure (0.15 MPa) for 7 min. Leaf hydraulic conductance (K_{leaf}, mmol m^{-2} s^{-1} MPa^{-1}) was calculated for five plants per treatment as the ratio between leaf transpiration (E, mmol m^{-2} s^{-1}) and water potential driving force ($\Delta\Psi_{leaf}$, MPa) as follows:

$$K_{leaf} = E/\Delta\Psi_{leaf}$$

E was taken from leaf gas exchange measurements, while $\Delta\Psi_{leaf}$ was calculated as the difference in water potential between bagged and unbagged leaves. Bagged leaves were wrapped with parafilm and tin foil for approximately 30 min before measuring water potential using a Scholander pressure chamber (Flexas et al., 2013).

Wood osmotic potential (π_{wood}, MPa) was measured in xylem parenchyma by cutting a 4 cm-long segment of the stem at a height of 40 cm and removing the bark. Wood material collected from five plants per treatment (n = 5) was transported to the laboratory, the bark was carefully removed, and the wood was cut into small pieces and pressed to extract the cellular liquid content using a metal garlic-press. The collected solution was used to saturate a 20 mm^2 filter paper disk and loaded in the thermocouple of a psychrometer connected to a laptop to monitor data acquisition. The psychrometer settings were the same as those previously employed for the Ψ_{stem}. After approximately 30 min, the equilibrium time in the chambers was reached, and the measurements were recorded.

A segment 4 cm in length was cut from the middle of the stem section from five plants per treatment (n = 5) and used to determine the relative water content (RWC_{wood}, %) using Eq. (1). After sampling, bark was carefully removed from the stem segments for fresh mass determination. The samples were rehydrated overnight. Once saturated, the mass was determined and the samples were oven-dried for 48 h before recording the dry weight. The rehydrated samples were not oversaturated because RWC_{wood} (%) did not increase above 100 (Sapes et al., 2021).

2.4. Pressure-volume curves

Leaf water potential isotherms (or pressure-volume curves, PV curves) were measured to estimate: (1) leaf water potential at the turgor loss point, Ψ_{tlp} (MPa); (2) relative water content at turgor loss point, RWC_{tlp} (%); (3) osmotic potential at full turgor, π_0; (4) bulk modulus of elasticity, ε_{max} (MPa); (5) apoplastic water fraction, AWF (%). Pressure–volume (PV) curves were measured on two twigs from five plants per treatment (n = 5) using the free-transpiration method (Tyree and Richter, 1982). Samples were collected at 19:00 and rehydrated overnight in a plastic bag for next-day measurements. After measuring the initial water potential (Ψ_{twig}, MPa) and mass, the samples were progressively dehydrated on the bench, and measurements were periodically repeated to obtain at least a 15-point curve with a linear relationship between water loss and Ψ_{twig}^{-1} ($R^2 > 0.95$). The samples were then oven dried for 72 h at 70 °C. Finally, Ψ_{twig}^{-1} was plotted *vs.* 100 – RWC (%) to obtain the PV curve, from which the parameters mentioned above were determined using a spreadsheet tool (Hinckley et al., 1980; Turner, 1988). No evidence of oversaturation for any of the samples used for the PV curves (the 'plateau effect') was found (Kubiske and Abrams, 1990).

2.5. Non-structural carbohydrates (NSCs)

Samples for NSCs were collected at 3 cm from the collar of five plants per treatment (n = 5), and the bark was removed, cutting a 1 cm-long segment, immediately sliced into thin sections with a razor blade, and dried overnight in an oven at 72 °C. The material (bark and phloem-free) was ground in liquid nitrogen and 30 mg was weighed for analysis. Soluble sugars and starch were extracted following the methodology of Landhäusser et al. (2018), with some modifications. After grinding the dried wood parenchyma, soluble sugars and starch were extracted separately. For sugars, we added 10 mL of ethanol (75 %) to 100 mg of the sample and extracted it at 60 °C for 30 min in a water bath. The samples were centrifuged, and the supernatant was collected, dried under vacuum, and resuspended in 1 mL of water for the analysis of soluble sugars by high-performance liquid chromatography (HPLC). To measure the starch content, the residual pellet from the soluble sugar extraction was washed with ethanol (75 %), dried, added to 1 mL of amyloglucosidase (0.5 % *w/v*), and incubated for 16 h at 50 °C. After incubation, the sample was centrifuged, and the supernatant was evaporated under vacuum and resuspended in 1 mL of water for injection. The analyses were performed by injecting 10 μL of the sample in a series 200 HPLC equipped with a 200-RI detector (PerkinElmer, Bradfrod, CT, USA), using a 7.7 × 300 mm, 8 μm Hi-Plex Ca (Agilent Technologies, USA) maintained at 85 ± 1 °C. The eluent was ultra-pure water at a flow rate of 0.5 mL min^{-1} during a 25-min run. Individual carbohydrates were identified by comparing retention times with those of authentic carbohydrate standards (Sigma-Aldrich, Milano, Italy), and quantification of the individual carbohydrates was performed using five-point calibration curves of glucose, fructose, and sucrose. Soluble sugars (glucose, fructose, and sucrose) are reported as mg/g DW, whereas starch is reported as the percentage of dry mass (g starch/g of DW x 100). Furthermore, the relative contribution of soluble sugars (sucrose, π_{sucr}; glucose, π_{gluc};fructose, π_{fruc}; and sum of soluble sugars, π_{SS}; MPa) to wood

osmotic potential (π_{wood}) was determined using the following formula (Gucci et al., 1997):

$$\pi_x = RT \times (RDW) \times C_x$$

where π_x indicates the contribution of individual each sugar to the osmotic potential (π, MPa), RDW is the relative dry weight at saturation (kg m^{-3}) calculated considering the TW and DW of RWC_{wood} (see the previous section), C is the molar concentration of each sugar (mol kg^{-1}), and the RT value at 25 °C is $-0.002479\ m^3\ MPa^{-1}\ mol^{-1}$. Furthermore, the percentage contribution of soluble sugars to the osmotic potential (%ss_π, %) was calculated as the ratio of π_{SS} to π_{wood}.

2.6. Gene expression

2.6.1. RNA extraction

Stems of three plants were cut into pieces of approximately 2 cm, frozen with liquid nitrogen, and stored at −80 °C. The bark was removed, and stems (bark and phloem-free) were dissected using a cryostat (−25 °C), producing 40 μm thick sections. Total RNA was extracted using a modified version of the protocol by Carvalho et al. (2015). Briefly, 200 mg of stem sections were transferred into a frozen 2-mL microtube, ground in liquid nitrogen, and homogenized using steel beads and Retsch Tissue Lyser (3 × 2 min at 20 Hz). Next, 1 mL of pre-warmed CTAB extraction buffer was added. Samples were vortexed, added with 2 % of 2-Mercaptoethanol, vortex again and incubated at 65 °C for 20 min, before being transferred to ice for 5 min. After the addition of 1 mL of chloroform/isoamyl alcohol (IAA) (24:1), they were vortexed and centrifuged at 14,000 rpm at 4 °C for 15 min. After two additional washes in chloroform/IAA (24:1), RNA was precipitated at −20 °C for 2 h by adding 0.1 mL of sodium acetate 3 M (pH 5.2) and 2.5 mL of cold ethanol (100 %). Samples were centrifuged for 30 min at 14,000 rpm at 4 °C to obtain a pellet of the precipitated RNA that was washed first with 250 μL of absolute cold ethanol at 4 °C, centrifuged at 14,000 rpm for 3 min, followed by a wash in ethanol 80 %. The pellet was air-dried, eluted with 20 μL of DEPC treated water and precipitation with LiCl 10 M was performed. The RNA pellet was washed with ethanol and eluted in 20 μL of RNase-free water. RNA samples were treated with DNase (TURBO™ DNase, Ambion) according to the manufacturer's instructions and quantified using a NanoDrop 1000 spectrophotometer.

2.6.2. Selection of candidate genes putatively associated to plant response to water stress and primer design

To assess remodeling in transcriptomic profiles, twenty genes were selected based on their putative involvement in the drought stress response of *Quercus spp*. Thirteen genes were selected based on the study by Madritsch et al. (2019), where they were identified as differentially regulated in response to drought stress. Specifically, one gene coding for a transcription factor putatively involved in ABA response (*bHLH30*), three genes coding for proteins related to ROS detoxification (*CYP75B1*, *NADK3*, *detox-like protein*), four protein-coding genes involved in remodeling of the plant cell wall during environmental stresses (*WAK*, *COMT*, *CCR*, *EXPA*), two genes (*AOS3, CUL1*) coding for proteins related to jasmonic acid biosynthesis and signaling, one gene (*CDR1*) coding for a protein involved in response to salicylic acid, a gene coding for a scopoletin glucosyltransferase (*TOGT*), a polyamine oxidase gene (*PAO1*) with a putative role in polyamine intracellular concentration, and an L-ascorbate oxidase gene (*AO*). Seven *Vitis vinifera* water stress-related proteins (Chitarra et al., 2014) were also identified in the transcriptome of *Q. ilex* using tblastx (e-value $<1e^{-5}$). Two additional genes coding for proteins putatively involved in ABA synthesis and response (*NCED1*, *NCED5*), one encoding for an aquaporin (*PIP2*), one gene encoding for a α-amylase (*BAM3*), and three genes coding proteins related to glucose 6P (*GPT1*) transport and sucrose synthesis, and transport (*SPS4*, *SUC27*) were selected.

Specific primers were designed using PRIMER3PLUS (http://www.bioinformatics.nl/cgi-bin/primer3plus/primer3plus.cgi) and tested for specificity to *Q. ilex* sequences using PRIMER BLAST (https://www.ncbi.nlm.nih.gov/tools/primer-blast/). Two genes, *RPL13* and TOPP2, encoding a 50S ribosomal protein L13 and ae serine/threonine-protein phosphatase PP1, respectively (Kotrade et al., 2019), were used as reference genes in the quantitative relative expression analysis (Tables SM1 and SM2).

2.6.3. RT-PCR and quantitative RT-PCR (RT-qPCR)

Primers for the two *Q. ilex* housekeeping genes, *i.e.*, *RPL13* and *TOPP2* were used to check for the absence of DNA contamination in RNA samples. One-step RT-PCR reactions were carried out in a final volume of 20 μL containing 4 μL of 5× buffer, 1 μL of 10 mM dNTPs, 0.5 μL of each primer (10 mM), 0.5 μL of enzyme mix and 1 μL of total RNA (diluted 1:3). The samples were incubated for 30 min at 50 °C followed by 15 min at 95 °C. Amplification reactions were run for 40 cycles at 94 °C for 30 s, 60 °C for 30 s, and 72 °C for 40 s. Amplicons were separated and visualized in ethidium bromide-stained agarose gels (1.5 % in TAE 0.5× buffer) using a Gel Doc™ EZ Imaging System (Bio-Rad, CA, USA).

For RT-qPCR, 500 ng of RNA was converted into cDNA using random primers and the Superscript™ II (Invitrogen). RT-qPCR was performed using the Rotor-Gene Q (Qiagen) apparatus. Reactions were carried out in a final volume of 15 μL with 7.5 μL of Rotor-GeneTM SYBR® Green Master Mix, 5.5 μL of a mix of forward and reverse primers (prepared by adding 16 μL of each primer at 10 μM stock concentration to 168 μL of water), and 2 μL of cDNA (diluted 1:3). The following PCR program was used:95 °C for 10 min, 40 cycles of 95 °C for 15 s, and optimal annealing temperature (Table SM1) for 30 s, ramp from 65 °C to 93 °C with a temperature increment of 0.5 °C, and a read plate every 2 s. Three biological and two technical replicates were used.

2.7. Anatomical analyses

For the anatomical analyses, on 10th August wood samples were collected at plant collars from three plants per treatment (R-WW and R-WS), fixed in formaldehyde, acetic acid, and alcohol 70 % (FAA, 1:1:1) for 24 h and then stored in alcohol 70 %. Sections (20 μm thick) were cut in a rotatory microtome (Olympus - Cut 4055, Tokyo, Japan) and treated with diverse staining protocols: Lugol for the detection of starch grains (Jensen, 1962); Toluidine Blue (1 %, − Feder and O'Brien, 1968) as a metachromatic stain used for the structural observations; Safranin (1 %) for the visualization of lignified cell walls; Ruthenium Red (0.01 %, Johansen, 1940) to localize pectin; and Alcian Blue (modified according to Arend et al., 2008) for the detection of mucilage. The slides were mounted in glycerin (70 %) and immediately analyzed using a Zeiss Axioplan microscope (Oberkochen, Germany) equipped with a Digital Net Camera Control Unit (Nikon, Eclipse E600, Japan). Measurements were conducted considering the final 50 % of the ring width to consider the wood produced during the rewatering period and taking into account the reduction in growth during the water stress period (see below). The selected tissue was classified into two zones, the zone around the largest vessels (Vessel Zone – VZ), in which vessel lumen area and frequency were measured, and the zone composed of fiber and few parenchyma cells (Fiber Zone – FZ), as reported in Fig. SM2 A and B. The fiber cell wall thickness (CW thickness, μm) was measured in the VZ and FZ according to Gärtner et al. (2015), considering the cell wall thickness of the two cells combined. Then, the percentage of cells with additional cell wall deposition (Add. CW, % of cells) was determined. All images were analyzed using ImageJ Pro (https://imagej.nih.gov/ij/).

Ring width was measured on WW and WS plants on 10th July (the sampling date at the end of the water stress treatment), assuming that it corresponded to the wood produced from 21st March, proposed as the date for the beginning of the vegetative period (Fig. SM3). Similarly, the ring width of R-WW and R-WS was measured on 10th August (sampling at the end of the rewatering period) assuming that it corresponded to the wood produced from 21st March to 10th August (Fig. SM3). The anatomical traits considered in this study were ring width (μm), vessel lumen area (μm^2), and vessel frequency (n° of vessels). The theoretical hydraulic conductivity (K_{th}) (kg s^{-1} MPa^{-1} m^{-1}) was calculated using the

Hagen–Poiseuille equation (Fan et al., 2012; Tyree et al., 1994; Zimmermann, 1983).

2.8. Statistics

For the physiological and NSCs data, a two-way ANOVA was applied, with differences between years and treatments as factors (Table SM3). As no differences were detected between the years, the data were combined, and only differences between treatments are presented in Figs. 1 and 3 (Table SM4). For the daily Ψ_{stem}, repeated measures ANOVA was applied (RM-ANOVA), considering plants measured under water stress (WW and WS plants) and rewatering (R-WW and R-WS plants) independently. Two-way ANOVA was applied for fiber cell wall thickness and percentage of cells with additional cell wall deposition, considering water treatments and ring zones as factors. For the PV curves and anatomical measurements (ring width, vessel lumen area, and frequency), a one-way ANOVA was applied with water treatment as the factor. Differences among the factors were tested using Tukey's test ($p < 0.05$). All statistical analyses were performed using Statistica software package (Stat Soft. Inc., Tulsa OK, USA). For gene expression analysis, data were analyzed using the comparative threshold cycle method (ΔΔCt) (Livak and Schmittgen, 2001). Ct of the target genes were normalized to the two established *Q. ilex* reference genes. Data ($2 - \Delta\Delta Ct$) were log2-transformed and normal distribution of data was tested through Shapiro–Wilk test by using R v.4.0.3. ANOVA and Tukey's test were then performed on raw values to assess the effect of water deficit and recovery (factors), and significant differences ($p \leq 0.05$) within conditions.

3. Results

3.1. Leaf physiological measurements

Water stress induced significant reductions in leaf gas exchanges, as marked declines in photosynthesis (P_n, −58 %) and stomatal conductance (g_s, −71 %) were observed in WS plants compared with control plants (Fig. 1A, B). After re-watering, P_n and g_s partially recovered but remained lower in R-WS compared to R-WW plants.

Chlorophyll fluorescence parameters were also affected by the water treatments. Both the maximum (F_v/fm) and actual efficiency (Φ_{PSII}) of photosystem II significantly decreased under water stress but did not differ between R-WS and R-WW plants, indicating a full photochemical efficiency recovery at the end of the rehydration period (Fig. 1C, D).

Leaf relative water content (RWC) was significantly lower in WS (~77 %) than in WW (~92 %) plants. The reduction in RWC persisted after rewatering (~88 % *vs.* ~92 %) (Fig. 1E). The delta of water potential ($\Delta\Psi$) was markedly higher in WS than in WW plants, whereas it did not vary significantly between R-WS and R-WW plants (Fig. 1F).

3.2. Plant hydraulics and aquaporin expression genes

The stem water potential (Ψ_{stem}) followed a typical daily trend in all treatments, with higher values in the morning, followed by a decrease in the central hours of the day and a recovery in the evening (Fig. 2). However, despite similar trends, WS plants always showed lower values of Ψ_{stem} compared to WW plants (Fig. 2A). Particularly, Ψ_{stem} did not significantly changed in WW and WS plants from pre-dawn to the morning. At ~16:00 h, Ψ_{stem} reached diurnal minimum values of ~ −1.3 Mpa in WW plants while it markedly dropped in WS plants reaching ~ − 4.6 MPa (Fig. 2A). In R-WS plants Ψ_{stem} was only slightly reduced compared to R-WW and significant changes were observed during the central hours of the day and in the late afternoon (Fig. 2B). Particularly, while the lowest values of Ψ_{stem} were ~ −1.0 MPa in R-WW plants, in R-WS plants the minimum values of Ψ_{stem} were ~ −1.6 MPa. Water stress induced an increase in PLC of approximately 15 % in WW plants and approximately 50 % in WS plants. Following rewatering, the PLC did not return to pre-stress values (Fig. 2C). The aquaporin gene *PIP2* (Fig. 2D) showed significantly higher transcript levels in WS than in

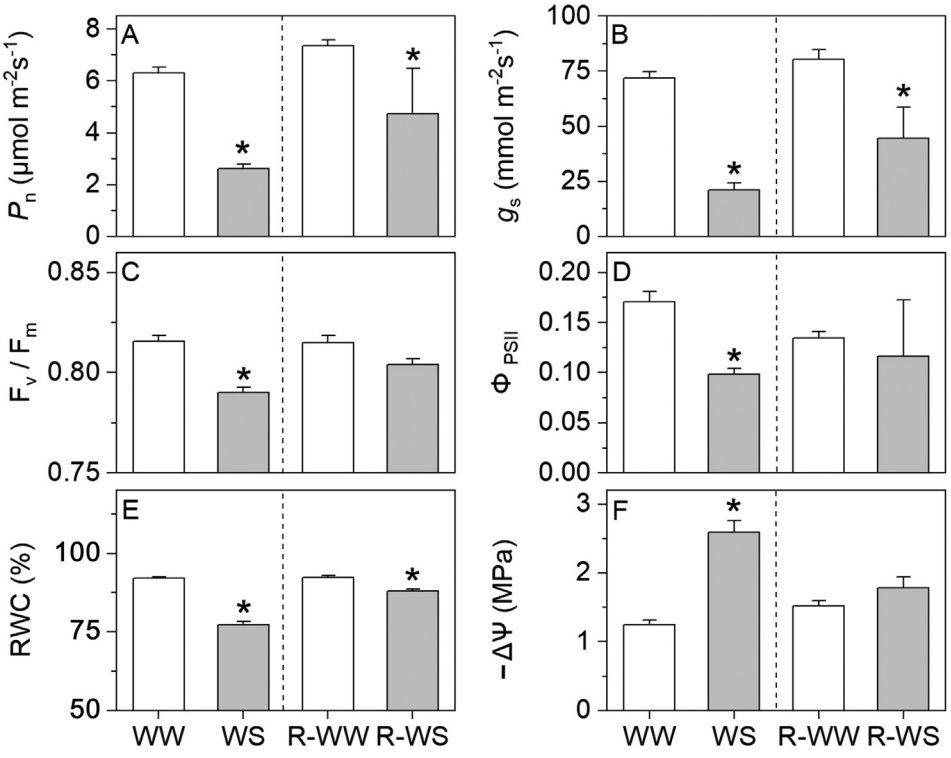

Fig. 1. Leaf physiological parameters comparing well-watered plants (WW) with water-stressed plants (WS) and well-watered plants (R-WW) with re-watered plants (R-WS): A) photosynthesis (P_n), B) stomatal conductance (g_s), C) maximum efficiency of photosystem II (F_v/fm), D) actual efficiency of photosystem II (Φ_{PSII}), E) leaf relative water content (RWC) and F) difference between leaf midday (Ψ_{MD}) and pre-dawn water potential (Ψ_{PD}) ($\Delta\Psi$). Mean ± SE ($n = 5$). Asterisks represent statistically significant differences ($p < 0.05$) between WW *vs* WS, and between R-WW *vs* R-WS. Detailed results of two-way ANOVA are reported in Tables SM1 and SM2.

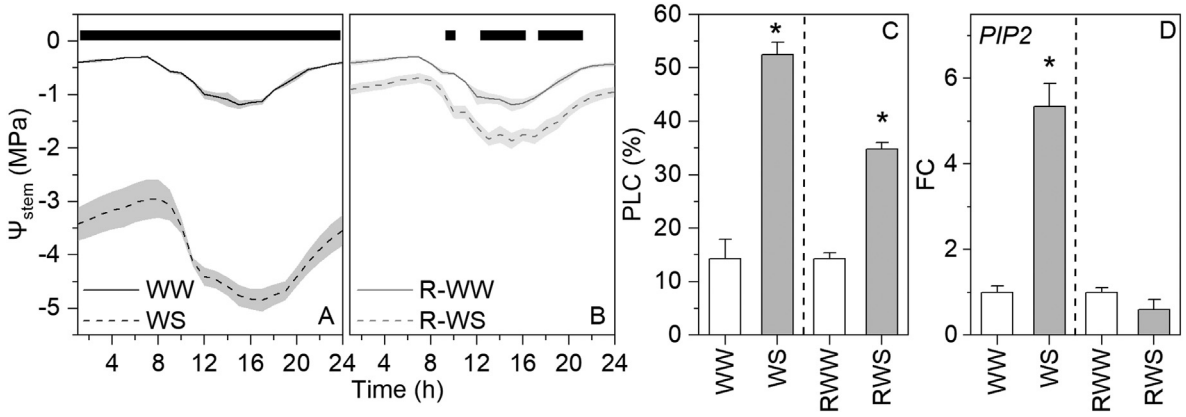

Fig. 2. A-B) Day course of stem water potential (Ψ_{stem}), C) percent loss of hydraulic conductivity (PLC) and D) *PIP2* expression, comparing well-watered plants (WW) with water-stressed plants (WS) and well-watered plants (R-WW) with re-watered plants (R-WS). Mean ± SE (n = 5). The bar on top of graphics A and B represents the hours of the day with significant statistical differences between treatments. Asterisks represent statistically significant differences ($p < 0.05$) between WW *vs* WS, and between R-WW *vs* R-WS. Detailed results of RM- and one-way ANOVA are reported in Tables SM1 and SM2.

WW plants, whereas no significant differences were observed between R-WS and R-WW plants.

Leaf hydraulic conductance (K_{leaf}) decreased in response to water stress, as the K_{leaf} values of WS plants corresponded to approximately 15 % of those recorded in WW plants. However, after re-watering, K_{leaf} did not fully recover, remaining 40 % lower in R-WS plants than in R-WW plants (Table 1). Water stress induced a remarkable decrease in the wood relative water content (RWC_{wood}) while no significant differences were found between R-WS and R-WW plants (Table 1). Similarly, wood osmotic potential (π_{wood}) was also reduced in WS compared to WW plants (−4.4 ± 0.14 MPa *vs* − 2.17 ± 0.16 MPa), with no differences observed after rewatering (Table 1). Finally, no differences in the percentage contribution of total soluble sugars to osmotic potential were found between WS and WW and R-WW and R-WS plants (%ss_{π}) (Table 1).

3.3. Non-structural carbohydrates' metabolism

At the end of the stress period, the amount of sucrose and percentage of starch decreased in WS compared to WW plants (Fig. 3A, D). In contrast, glucose and fructose content increased in WS compared to WW plants, whereas no differences in the levels of these sugars were detected between R-WS and R-WW plants (Fig. 3B, C). Stem structural analysis, highlighting the starch grains, confirmed the quantitative data (Fig. 3E-G). In R-WW plants, starch was abundant inside the VZ, FZ, and ray and was distributed inside parenchymatic cells (Fig. 3E). WS plants showed almost no starch accumulation in the stem tissue (Fig. 3E). After re-watering, however, starch grains were again visualized, mostly accumulated in the parenchyma cell near the VZ and in the ray but hardly found in the parenchyma cells of FZ (Fig. 3G).

The genes coding for a β-amylase (*BAM3*) and a putative sucrose-phosphate synthase (*SPS4*) were upregulated in WS plants (Fig. 4A, B). In contrast, transcripts corresponding to two homologous grapevine genes coding for a plastidic glucose-6P symporter (*GPT1*) and a sucrose transporter (*SUC27*) were downregulated in WS plants (Fig. 4C, D). However, transcripts linked to sugar mobilization showed no significant differences between R-WW and R-WS plants (Fig. 4).

3.4. Pressure-volume curves

Pressure-volume (PV) curve-derived parameters were affected by the different water treatments (Table 2). In particular, water potential at turgor loss point (Ψ_{tlp}) and osmotic potential at full turgor (π_0) were significantly lower in WS plants than in WW plants (Table 2). However, no differences were observed between R-WW and R-WS plants for Ψ_{tlp} and π_0. Conversely, the relative water content al turgor loss point (RWC_{tlp}) did not differ between WS and WW, while it was significantly reduced in R-WS compared to R-WW. In addition, higher values of the bulk modulus of tissue elasticity (ε) were found in WS than in WW plants, whereas ε was significantly lower in R-WS than in R-WW plants. Finally, WS plants showed a lower apoplastic water fraction (AWF) than WW plants. Conversely, R-WS plants showed lower but not significantly different values of AWF compared to R-WW plants.

3.5. Wood anatomy and cell wall related genes

The results of cell wall related gene expression showed an upregulation of *EXPA*, coding for a putative expansin, and *CCR*, coding for a cinnamoyl-CoA reductase 1 involved in lignin biosynthesis, in WS plants (Fig. 5). Finally, another gene involved in lignin synthesis, *COMT,* was downregulated under water stress conditions (Fig. 5).

Staining specificity confirmed the lignin matrix of the secondary cell wall (CW) (Fig. 6 A1-A2 and B1-B2). Additional deposition of material on the cell wall (Add. CW) was observed in R-WS plants occupying the entire cell lumen and was composed of various compounds, including phenolics (Fig. 6 B1 *vs* A1, B2 *vs.* A2), pectins (Fig. 6 B3 *vs* A3), and mucilage (Fig. 6 B4 *vs* A4). However, the effect of water treatment on CW thickness and the percentage of Add. CW was different when considering the fiber (FZ) and vessel (VZ) zones separately (Table 3). In the FZ higher values of

Table 1
Leaf hydraulic conductance (K_{leaf}), wood relative water content (RWC_{wood}), wood osmotic potential (π_{wood}) and the contribution of total soluble sugars to osmotic potential (π_{SS}) comparing well-watered plants (WW) with water-stressed plants (WS) and well-watered plants (R-WW) with re-watered plants (R-WS). Mean ± SE ($n = 5$). Asterisks represent statistically significant differences ($p < 0.05$) between WW *vs* WS, and between R-WW *vs* R-WS. Detailed results of one-way ANOVA are reported in Table SM3. Details of the contribution to osmotic potential of the single soluble sugars are reported in Table SM5.

Parameter	WW	WS	*P*	R-WW	R-WS	*P*
K_{leaf} (mmol m^{-2} s^{-1} MPa^{-1})	3.52 ± 0.50	0.53 ± 0.08	*	3.77 ± 0.47	1.84 ± 0.37	*
RWC_{wood} (%)	91.4 ± 0.02	78.8 ± 0.03	*	91.8 ± 0.02	89.7 ± 0.01	*n.s*
π_{wood} (MPa)	−2.17 ± 0.16	−4.40 ± 0.14	*	−1.68 ± 0.10	−2.17 ± 0.21	n.s
% π_{SS} (%)	14.66 ± 1.15	8.63 ± 0.50	*	17.45 ± 9.38	13.46 ± 1.04	*

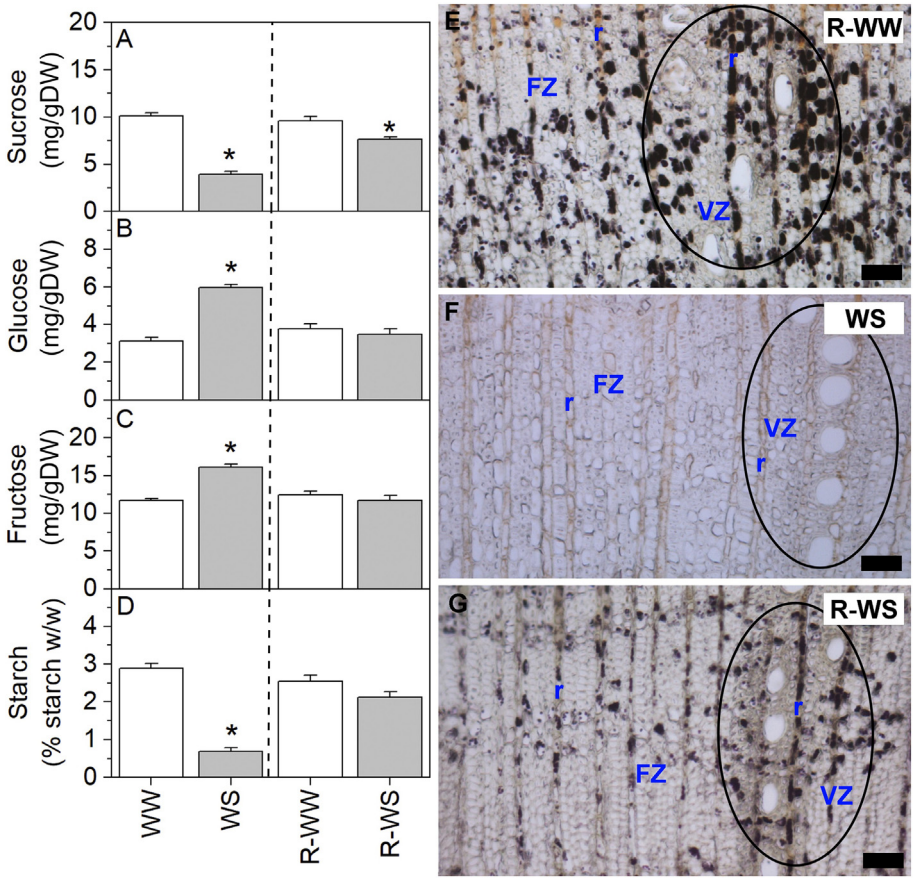

Fig. 3. A - D) Content of non-structural carbohydrates (sucrose, glucose, fructose and starch) comparing well-watered plants (WW) with water-stressed plants (WS) and well-watered plants (R-WW) with re-watered plants (R-WS). Mean ± SE (n = 5). Asterisks represent statistically significant differences ($p < 0.05$) between WW *vs* WS, and between R-WW *vs* R-WS. Detailed results of two-way ANOVA are reported in Tables SM1 and SM2. E – G) Analysis of *Q. ilex* stem showing the distribution of starch grains observed as black rounded structures stained by Lugol solution in well-watered plants (E), water-stressed plants (F) and re-watered plants (G). The accumulation of starch occurs in parenchyma cells, mainly in the ray parenchyma cells (r) around the vessel zone (VZ - ellipse) compared to the fiber zone (FV). Bars = 200 μm.

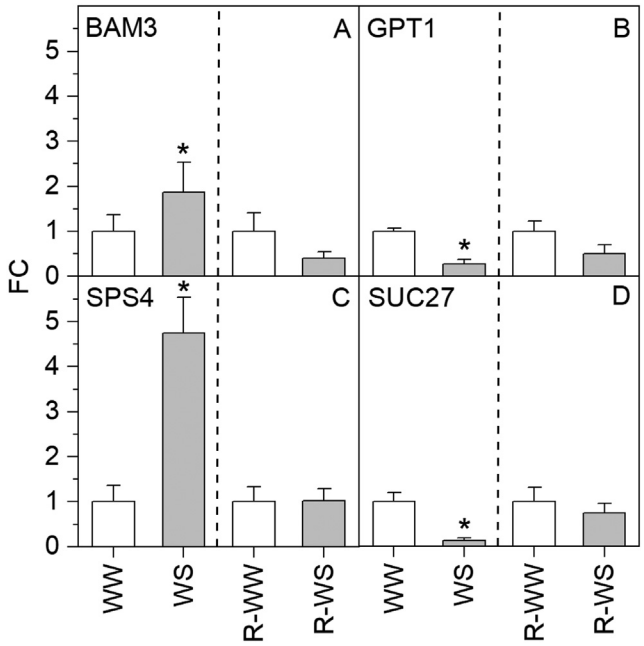

Fig. 4. *BAM3, GPT1, SPS4,* and *SUC27* expression comparing well-watered plants (WW) with water-stressed plants (WS) and well-watered plants (R-WW) with re-watered plants (R-WS). Mean ± SE ($n = 3$). Asterisks represent statistically significant differences ($p \leq 0.05$) between WW *vs* WS, and between R-WW *vs* R-WS.

CW thickness and % of Add. CW were observed both in WS and R-WS plants compared to controls, while in the VZ differences between treatments were observed only after re-watering (Table 3). The ring width was reduced by the water stress treatment (Fig. SM3). In addition, after re-watering the number of vessels increased significantly but their area was lower in R-WS plants compared to controls (Fig. SM3).

4. Discussion

4.1. Reduction of leaf gas exchanges under water stress led to NSCs consumption without preventing loss of hydraulic conductivity

Our results showed that the water stress treatment applied to holm oak seedlings was severe, as both leaf gas exchange and chlorophyll fluorescence parameters were strongly reduced, with values of F_v/fm close to irreversible leaf damage (Flexas and Medrano, 2002; Peguero-Pina et al., 2009) (Fig. 1). In particular, both P_n and g_s were reduced by approximately 70 % in WS plants compared with WW plants, whereas intercellular CO_2 concentration (C_i) was reduced by only 28 %, indicating both biochemical and diffusional limitations of photosynthesis under water stress (Fig. 1; Tables SM3 and SM4). However, stomatal closure was not sufficient to prevent a dramatic decline in both leaf Ψ_{MD} and RWC beyond Ψ_{tlp} and RWC_{tlp} in WS plants compared with the controls (Figs. 1 and SM4, Table 1). Moreover, we observed a significant reduction in AWF (Table 2) concomitantly with an increase in the bulk elastic modulus (ε), indicating harder and less elastic cell walls in WS plants compared with WW plants (Saito et al., 2006; Salleo et al., 1997).

Table 2
Pressure-volume curve parameters: water potential at turgor loss point (Ψtlp), relative water content at turgor loss point (RWC_{tlp}), osmotic potential at full turgor (π0), bulk modulus of elasticity (ε_{max}) and apoplastic water fraction (AWF) comparing well-watered plants (WW) with water-stressed plants (WS) and well-watered plants (R-WW) with re-watered plants (R-WS). Mean ± SE (n = 5). Asterisks represent statistically significant differences ($p < 0.05$) between WW *vs* WS, and between R-WW *vs* R-WS. Detailed results of one-way ANOVA are reported in Table SM3.

Parameter	WW	WS	*P*	R-WW	R-WS	*P*
Ψ_{tlp} (MPa)	−2.32 ± 0.09	−3.89 ± 0.22	*	−2.25 ± 0.13	−2.73 ± 0.18	*n.s*
RWC_{tlp} (%)	89.4 ± 0.72	85.6 ± 2.61	*n.s*	90.9 ± 1.50	79.6 ± 2.64	*
π_0 (MPa)	−1.88 ± 0.11	−3.47 ± 0.21	*	−1.86 ± 0.10	−1.72 ± 0.26	*n.s*
ε_{max} (MPa)	11.9 ± 0.75	19.7 ± 3.11	*	12.8 ± 1.66	5.0 ± 1.23	*
AWF (%)	0.73 ± 0.23	0.40 ± 0.52	*	0.73 ± 0.18	0.68 ± 0.38	*n.s*

Our data showed that, under severe water stress, *Q. ilex* leaves experienced a significant loss in hydraulic conductance, as K_{leaf} of WS plants accounted for approximately 15 % of that of WW plants (Table 1). The observed reduction in K_{leaf} was also accompanied by a Ψ_{stem} drop of approximately −4.6 MPa and an increment in PLC values to approximately 50 % in WS plants (Fig. 2A and C, Table 1). These values of xylem vulnerability to embolism are very close to those found in previous studies on *Q. ilex* potted saplings exposed to severe water stress, reporting a PLC of 50 % at a water potential between −4.5 and − 5.5 MPa (Peguero-Pina et al., 2014; Resco de Dios et al., 2020). Our findings suggest a lack of hydraulic segmentation, in accordance with recent studies reporting that *Q. ilex* leaves and stems are equally vulnerable to drought-induced embolism (Alonso-Forn et al., 2021; Peguero-Pina et al., 2015; Skelton et al., 2018). Indeed, evergreen sclerophyll species exhibit a conservative leaf strategy that relies on high leaf mass per area, long time span, and high construction costs (Flexas et al., 2013; Martin-StPaul et al., 2017; Skelton et al., 2018; Smith-Martin et al., 2020). Nevertheless, further studies are needed to track embolism propagation between stems and leaves of this species. For example, it is possible that higher levels of stress may lead to the occurrence of higher degrees of embolism in leaves *versus* stems because of the steeper water potential gradients that would occur with higher levels of transpiration, as reported by Limousin et al. (2022).

The increase in PLC under reduced soil water availability may also have triggered the upregulation of aquaporins *PIP2* in WS plants (Fig. 2D). Previous studies have found that *PIP2* aquaporin genes are involved in the drought response, with a specific expression in vessel-associated cells in walnut trees and grapevine petioles (Lopez et al., 2003; Chitarra et al., 2014). Our data support previous evidence that *PIP2* aquaporins facilitate water movement across the plasma membrane in wood parenchyma, thus assisting the radial movement of water from living tissues to xylem vessels (Cao et al., 2014; Lopez et al., 2013; Pfautsch et al., 2015). The water stress-induced decrease in P_n resulted in a decrease in NSCs concentration in the wood parenchyma, as previously reported by Brunetti et al. (2019) and Tomasella et al. (2019b). When carbon shortage occurs, multiple enzymes may break down starch into soluble sugars, such as α and β amylases (Thalmann and Santelia, 2017). In our study, the observed reduction in starch content was likely due to its enhanced degradation (Fig. 3). Indeed, *BAM3*, a β-amylase gene homologous to *BAM3* in grapevine (Chitarra et al., 2014; Perrone et al., 2012) and *Arabidopsis* (Fulton et al., 2008), was upregulated in WS plants, along with a concurrent increase in soluble carbohydrates and an almost complete disappearance of starch grains in parenchyma cells (Figs. 3 and 4). Previous studies have shown that β-amylase upregulation is driven by abscisic acid (ABA) (Thalmann and Santelia, 2017). Therefore, the upregulation of *NCED5* and *NCED1* in WS plants could have led to an increase in ABA biosynthesis that, in turn, may have triggered starch degradation in the woody tissue (Chitarra et al., 2014; Brunetti et al., 2019). A possible involvement of ABA in holm oak response to water stress was also indicated by the ABA-responsive gene expression of the bHLH30 transcription factors (Fig. SM5) (Madritsch et al., 2019). In addition, a lower sucrose content was observed along with a decrease in the expression of *SUC27*, an H^+-dependent sucrose transporter (Fig. 4). Downregulation of *SUC27* has been previously reported in grape petioles (Perrone et al., 2012), suggesting that under severe water stress, the main provision of sugars to vessel-associated cells may be derived from starch degradation and not from phloem unloading. Therefore, downregulation of *SUC27* may have reduced the efflux of sucrose to the apoplast, thus sustaining cellular metabolism under water stress (Payyavula et al., 2011). In support of this hypothesis, the *GPT1* gene was also found to be downregulated in WS plants, indicating a limitation in glucose transport and accumulation of starch reserves in the woody tissue (Noronha et al., 2018). The low wood sucrose content may have triggered the upregulation of a sucrose synthase gene (*SPS4*) (Fig. 4). However, since sucrose accumulation was not observed, we suggest a high catabolism of this sugar due to the activity of apoplastic invertases, which, even if not directly examined in our study, are usually upregulated under water stress conditions and low pH (Pagliarani et al., 2019). Considering that wood is an important sink tissue for starch accumulation, we can surmise that the severe stress conditions reached in our experiment limited photosynthesis and induced the depletion of carbohydrate reserves that were used to maintain respiration and provide energy for cellular metabolism (Galiano et al., 2012; Noronha et al., 2018; Rodríguez-Calcerrada et al., 2021).

These results imply that soluble sugars play a negligible role in providing the osmotic force to maintain cell turgor and regulate *Q. ilex* water balance (Resco de Dios and Gessler, 2021), as also highlighted by the calculation of ss_π which was lower than <20 % in both WS and WW plants (Table 1, Table SM5). Accordingly, WS plants showed passive osmotic adjustment in wood parenchyma cells because the significant reduction in π_{wood} was accompanied by a decrease in RWC_{wood}, suggesting that tissue dehydration was the main cause of the observed accumulation of solutes (Table 1).

The expression of the CCR1 gene, which is involved in the lignification of interfascicular fibers and xylem vessels, suggests that water stress also caused the activation of lignin biosynthesis in wood parenchyma, as previously reported in leaves (Fig. 5) (Srivastava et al., 2015; Vanholme et al., 2010). In addition, under water stress, a gene coding for an α-expansin protein (*EXPA*) weas upregulated (Fig. 5). Expansin proteins mediate cell wall loosening, and several studies have shown that upregulation of α-expansin gene expression results in a higher water retention ability under drought conditions, although the possible mechanisms remain unclear (Jin et al., 2020; Tenhaken, 2015; Wu et al., 2001). Finally, water stress may have activated protective adjustments against oxidative stress in wood parenchyma (Fonti et al., 2013). In particular, our results suggest that prolonged water deprivation induces the expression of *NADK3* and *CYP75B1* genes,

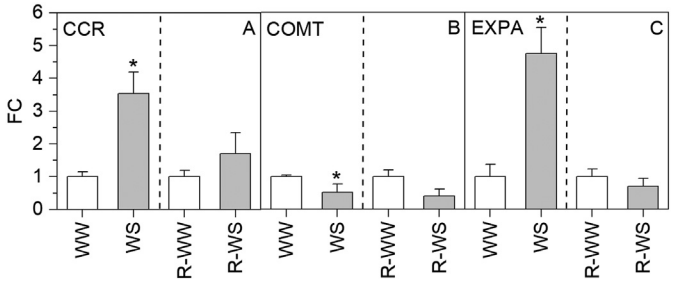

Fig. 5. *CCR, COMT,* and *EXPA* expression in *Q. ilex* comparing well-watered plants (WW) with water-stressed plants (WS) and well-watered plants (R-WW) with re-watered plants (R-WS). Mean ± SE (n = 3). Asterisks represent statistically significant differences ($p < 0.05$) between WW *vs* WS, and between R-WW *vs* R-WS.

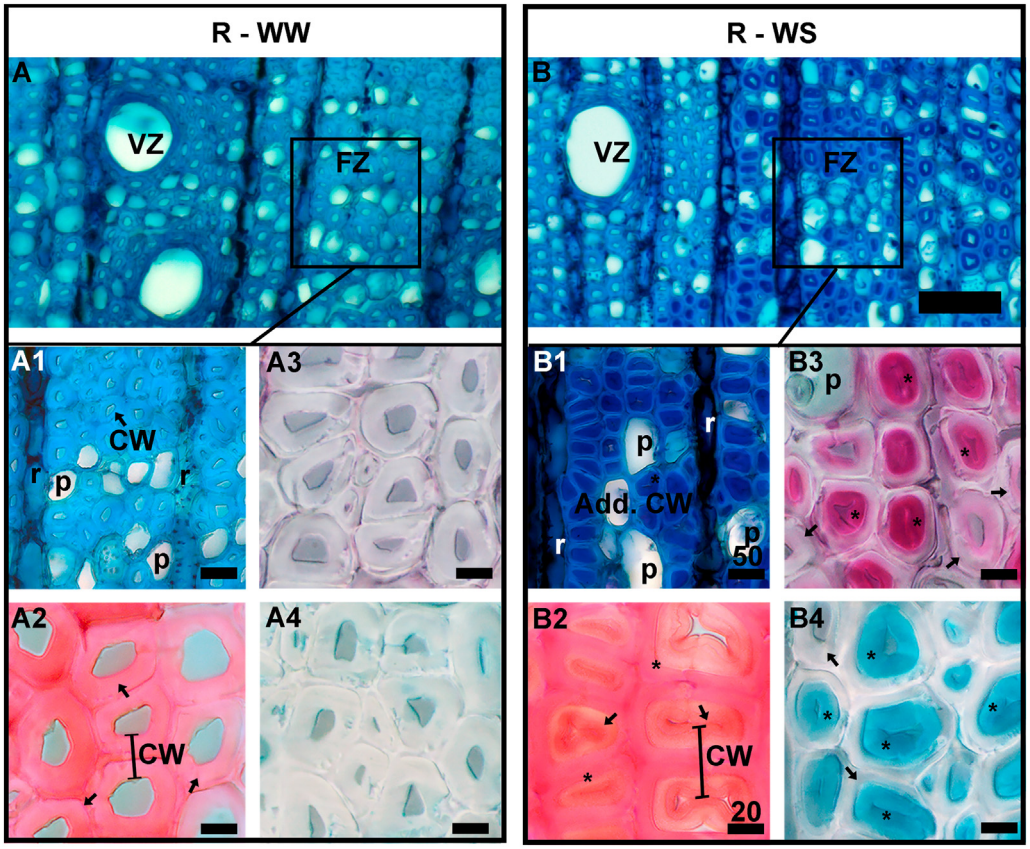

Fig. 6. A – B) Anatomical observations of *Q. ilex* stem in well-watered (A / R-WW) and re-watered (B / R-WS) plants. In the fiber zone (FZ), additional deposition of material on the cell wall (Add. CW/ asterisks) was found in R-WS plants compared to R-WW plants (CW – arrows), with phenolic compounds identified by the dark-blue/purplish colour of the toluidine blue (B1 *vs.* A1), lignin matrix identified by the safranin (B2 *vs.* A2), pectin highlighted in pink by the ruthenium red (B3 *vs.* A3), and mucilage dyed in light blue by the Alcian blue stain (B4 *vs.* A4).

which are involved in the production of NADP(H) and flavonoids, respectively, and play a primary role in the scavenging of reactive oxidative species (Fig. SM5) (Kotrade et al., 2019; Madritsch et al., 2019). The upregulation of two genes (*AOS3* and *CUL1*) encoding proteins putatively involved in jasmonic acid biosynthesis supports previous hypotheses regarding the involvement of this hormone in the biosynthesis of antioxidant compounds (Fig. SM5) (Kim et al., 2006; Nagels Durand et al., 2016; Yuan et al., 2017).

4.2. The recovery of wood NSCs reserves was not accompanied by a full restoration of hydraulic conductivity after rewatering

Our findings suggest that the *Q. ilex* photosynthetic apparatus is highly resilient to water stress, as F_v/fm and Φ_{PSII} fully recovered after thirty days of rewatering (Fig. 1). However, only partial recovery of leaf gas exchange and leaf hydraulic traits was observed in R-WS plants compared with R-WW plants, indicating that the incomplete recovery of P_n was caused by the persistence of stomatal limitations (Fig. 1, Table SM4) (Peguero-Pina et al., 2018). In addition, leaf water parameters (Ψ_{MD} and RWC) remained lower in R-WS plants than in R-WW plants, indicating a lack of leaf hydraulic recovery owing to xylem embolism persistence (Fig. 1; SM4) (Creek et al., 2018). Accordingly, K_{leaf} and PLC did not show complete recovery even after thirty days of rewatering, implying that the restoration of xylem conductivity was primarily due to new xylem growth rather than active xylem refilling (Choat et al., 2015; Rehschuh et al., 2020) (Fig. 2; Table 1). At the same time, residual xylem embolism and the lack of hydraulic recovery may explain the inability of *Q. ilex* seedlings to restore stomatal conductance, highlighting the close relationship between leaf gas exchange and hydraulic functionality. This may indicate that, in this species, the stomatal aperture is mainly driven by water potential rather than by other mechanisms, such as abscisic acid signaling and accumulation, as previously suggested by Peguero-Pina et al. (2018).

After rewatering, a higher number of vessels with a lower diameter was found in R-WS plants than in R-WW plants, suggesting that the variation in hydraulic conductivity may be related to changes in conduit size, as revealed by the significant reduction in K_{th} (Tables SM3 and SM4) (Corcuera et al., 2004; De Micco et al., 2008). Indeed, the occurrence of frequent small vessels throughout the entire ring in *Q. ilex* represents a strategy to cope with unfavourable conditions (freeze events in winter and drought periods in summer) because small vessels are less susceptible to cavitation and embolism (Campelo et al., 2010; Cavender-Bares et al., 2005). Other important anatomical modifications in cell wall thickness and composition

Table 3
Summary of the results of two-way ANOVA on cell wall thickness (CW) and additional CW (Add. CW) in fiber (FZ) and vessel (VZ) zones of *Q. ilex* plants. Letters indicate significant differences among treatments ($p < 0.05$).

	WW		WS		R-WW		R-WS	
	VZ	FZ	VZ	FZ	VZ	FZ	VZ	FZ
CW thickness (μm)	6.23 ± 0.03d	6.89 ± 0.07c	6.47 ± 0.14c	9.66 ± 0.31a	5.94 ± 0.06d	7.53 ± 0.14b	7.03 ± 0.15bc	9.36 ± 0.06a
Add. CW (% of cells)	14.6 ± 0.19d	31.68 ± 2.89c	24.89 ± 5.7c	72.79 ± 6.08a	13.63 ± 2.62d	46.73 ± 1.88b	37.50 ± 4.33bc	81.74 ± 3.74a

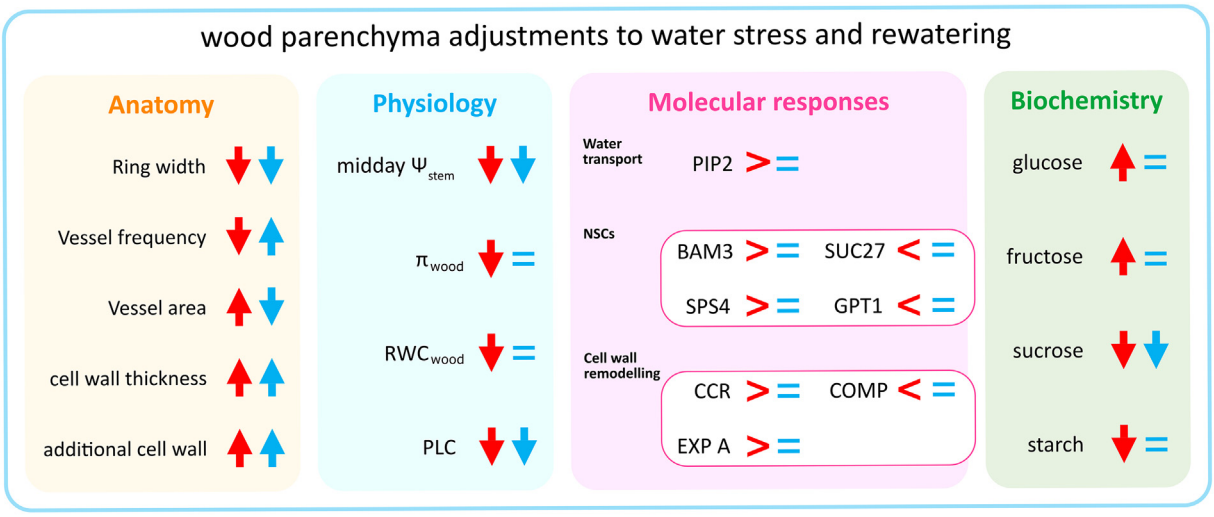

Fig. 7. Figure summarizing the anatomical, physiological, molecular and biochemical responses of *Q. ilex* to thirty days of water stress and thirty days of rewatering. Red symbols were used to compare water stress plants (WS) to well-watered (WW) while blue symbols were used to compare re-watered plants (RW) to re-watering (R-WW). Upward and downward arrows indicate an increase or a decrease, respectively, in the corresponding values of treated plants (WS and R-WS) compared to the control plants (WW and R-WW). The symbols (>) and (<) indicate an up-regulation or a downregulation, respectively, in gene expressions of treated plants (WS and R-WS) compared to control plants (WW and R-WW); while the symbol (=) indicates no differences in gene expression comparing WS plants to WW plants, and R-WS plants to R-WW plants. Abbreviation: Ψ_{stem}, xylem water potential; π_{wood}, wood osmotic potential; RWC_{wood}, wood relative water content; PLC, percentage loss of hydraulic conductivity; NSCs, non-structural carbohydrates.

were also observed under rewatering conditions (Fig. 6). The composition of the additional cell wall observed in *Q. ilex* wood parenchyma fibers can be identified as gelatinous fibers (Fig. 6B), mainly composed of non-lignified substances such as pectin and hemicelluloses, and characterized by greater thickness, lower density, and loosening appearance compared to the cell wall secondary layers (Ghislain and Clair, 2017; Piva et al., 2019; Western, 2012), and is usually more abundant in roots or in tension wood (Bowling and Vaughn, 2008; Piva et al., 2020). Indeed, pectin has been shown to play a crucial role in modulating cell wall structure, helping recovery from severe drought episodes (Le Gall et al., 2015). In our study, the formation of gelatinous fibers, is suggested as a short-term water storage structure that helps *Q. ilex* recover from water stress (Carlquist, 2014), and it can be an important anatomical marker of drought episodes (Cabane et al., 2012). In fact, the downregulation of a putative *COMT*, coding a caffeic acid *o*-methyltransferase, induced by water stress in wood parenchyma may have generated the changes in the lignin chemical structure observed after rewatering, that led to different proportions of the three monomers p-coumaryl, coniferyl and sinapyl alcohol and, consequently, in the G-/S-type ratio of lignin (guaiacyl/ syringyl) (Figs. 5 and 6) (Chanoca et al., 2019; Lu et al., 2019). At the same time, we may surmise that the involvement of *EXPA* in cell wall remodeling may be related to the observed changes in cell wall composition of fibers, in particular to the accumulation of substances that undergo considerable swelling upon hydration contributing to wood parenchyma water storage (Jupa et al., 2016).

Finally, in accordance with our second hypothesis, the fresh assimilated carbon derived from the partial recovery of P_n led to the accumulation of new starch reserves in the wood parenchyma cells, particularly those surrounding the xylem conduits (Fig. 3). Similar results have also been reported for this species under both greenhouse and field conditions (Aguadé et al., 2015; Rodríguez-Calcerrada et al., 2017; Peguero-Pina et al., 2018). Our findings indicate that, in *Q. ilex* seedlings, thirty days of rewatering were sufficient to restore NSCs reserves and growth rates (Figs. 3 and SM3, Table SM4) and that the carryover effects of water stress were primarily caused by hydraulic dysfunction (Fig. 2).

5. Conclusion

In this study, we provide new insights into the multiple mechanisms responding to severe water stress and rewatering in the wood parenchyma of holm oak seedlings (Fig. 7). Our study demonstrated that severe water stress critically impaired plant metabolic and hydraulic functioning. Indeed, the maintenance of high carbon demands for growth and respiration, in parallel with a reduction in photosynthesis, causes NSCs depletion in the wood parenchyma of the WS plants. After thirty days of rewatering, a lack of leaf hydraulic recovery due to xylem embolism persistence was observed, causing an incomplete restoration of leaf gas exchanges. However, the partial re-increase in photosynthetic rates enabled the storage of new wood starch reserves, particularly in cells surrounding the vessels. Several anatomical changes related to the formation of new vessels as well as changes in the wall thickness and composition of wood parenchyma cells were also observed, assisting in the recovery of the plant water storage capacity. Based on our findings, we suggest that severe water stress results in hydraulic impairment of *Q. ilex* seedlings, and that recovery is dependent on the regrowth of new vessels. Thus, water stress carryover effects may affect plant resilience, compromising holm oak physiological performances under recurrent and severe drought events.

CRediT authorship contribution statement

Conceptualization: C. Brunetti, A. Gori; Investigation: C. Brunetti, A. Gori, F. Alderotti, D. Pasquini, B. Baesso Moura, F. Sillo, R. Balestrini; Methodology: C. Brunetti, A. Gori, F. Alderotti, D. Pasquini, B. Baesso Moura, F. Sillo, R. Balestrini; Formal analysis: B. Baesso Moura, F. Sillo, F. Alderotti; Data curation: C. Brunetti, A. Gori, F. Alderotti, D. Pasquini, B. Baesso Moura, F. Sillo, R. Balestrini; Formal analysis: C. Brunetti, A. Gori, F. Alderotti, D. Pasquini, B. Baesso Moura, F. Sillo, R. Balestrini; F. Ferrini, M. Centritto. Writing – original draft: C. Brunetti, A. Gori, R. Balestrini; Writing – review & editing: all the authors. Supervision: C. Brunetti, A. Gori, M. Centritto, R. Balestrini; Resource acquisition: M. Centritto, F. Ferrini.

Funding information

The authors declare that no funds, grants, or other support were received during the preparation of this manuscript.

Data availability

All data are included in the manuscript and in supplementary materials.

Declaration of competing interest

The authors declare that they have no known competing financial interests or personal relationships that could have appeared to influence the work reported in this paper.

Appendix A. Supplementary data

Supplementary data to this article can be found online at https://doi.org/10.1016/j.scitotenv.2023.163124.

References

Aguadé, D., Poyatos, R., Rosas, T., Martínez-Vilalta, J., 2015. Comparative drought responses of Quercus ilex L. and Pinus sylvestris L. in a montane forest undergoing a vegetation shift. Forests 6 (8), 2505–2529. https://doi.org/10.3390/f6082505.

Allen, C.D., Macalady, A.K., Chenchouni, H., Bachelet, D., McDowell, N., Vennetier, M., et al., 2010. A global overview of drought and heat-induced tree mortality reveals emerging climate change risks for forests. For. Ecol. Manag. 259, 660–684. https://doi.org/10.1016/j.foreco.2009.09.001.

Alonso-Forn, D., Peguero-Pina, J.J., Ferrio, J.P., Mencuccini, M., Mendoza-Herrer, Ó., Sancho-Knapik, D., Gil-Pelegrín, E., 2021. Contrasting functional strategies following severe drought in two Mediterranean oaks with different leaf habit: Quercus faginea and Quercus ilex subsp. Rotundifolia. Tree Physiol. 41 (3), 371–387. https://doi.org/10.1093/treephys/tpaa135.

Anderegg, W.R.L., Konings, A.G., Trugman, A.T., Yu, K., Bowling, D.R., Gabbitas, R., et al., 2018. Hydraulic diversity of forests regulates ecosystem resilience during drought. Nature 561, 538–541. https://doi.org/10.1038/s41586-018-0539-7.

Anderegg, W.R.L., Trugman, A.T., Badgley, G., Konings, A.G., Shaw, J., 2020. Divergent forest sensitivity to repeated extreme droughts. Nat. Clim. Chang. 10, 1091–1095. https://doi.org/10.1038/s41558-020-00919-1.

Arend, M., Fromm, J., 2007. Seasonal change in the drought response of wood cell development in poplar. Tree Physiol. 27, 985–992. https://doi.org/10.1093/treephys/27.7.985.

Arend, M., Muninger, M., Fromm, J., 2008. Unique occurrence of pectin-like fibrillar cell wall deposits in xylem fibres of poplar. Plant Biol. 10, 763–770. https://doi.org/10.1111/j.1438-8677.2008.00082.x.

Bowling, A.J., Vaughn, K.C., 2008. Immunocytochemical characterization of tension wood: gelatinous fibers contain more than just cellulose. Am. J. Bot. 95, 655–663. https://doi.org/10.3732/ajb.2007368.

Brodribb, T.J., Powers, J., Cochard, H., Choat, B., 2020. Hanging by a thread? Forests and drought. Science 368, 261–266. https://doi.org/10.1126/science.aat7631.

Brunetti, C., Loreto, F., Ferrini, F., Gori, A., Guidi, L., Remorini, D., et al., 2018. Metabolic plasticity in the hygrophyte Moringa oleifera exposed to water stress. Tree Physiol. 38, 1640–1654. https://doi.org/10.1093/treephys/tpy089.

Brunetti, C., Gori, A., Marino, G., Latini, P., Soboley, A.P., Nardini, A., et al., 2019. Dynamic changes in ABA content in water-stressed Populus nigra: effects on carbon fixation and soluble carbohydrates. Ann. Bot. 124, 627–643. https://doi.org/10.1093/aob/mcz005.

Brunetti, C., Savi, T., Nardini, A., Loreto, F., Gori, A., Centritto, M., 2020. Changes in abscisic acid content during and after drought are related to carbohydrate mobilization and hydraulic recovery in poplar stems. Tree Physiol. 40, 1043–1057. https://doi.org/10.1093/treephys/tpaa032.

Cabane, M., Afif, D., Hawkins, S., 2012. Lignins and abiotic stresses. Advances in Botanical Research. Elsevier, pp. 219–262 https://doi.org/10.1016/B978-0-12-416023-1.00007-0.

Camarero, J.J., Sangüesa-Barreda, G., Vergarechea, M., 2016. Prior height, growth, and wood anatomy differently predispose to drought-induced dieback in two Mediterranean oak species. Ann. For. Sci. 73, 341–351. https://doi.org/10.1007/s13595-015-0523-4.

Campelo, F., Nabais, C., Gutiérrez, E., Freitas, H., García-González, I., 2010. Vessel features of Quercus ilex L. Growing under Mediterranean climate have a better climatic signal than tree-ring width. Trees 24, 463–470. https://doi.org/10.1007/s00468-010-0414-0.

Cao, X., Jia, J., Zhang, C., Li, H., Liu, T., Jiang, X., et al., 2014. Anatomical, physiological and transcriptional responses of two contrasting poplar genotypes to drought and re-watering. Physiol. Plant. 151, 480–494.

Carlquist, S., 2014. Fibre dimorphism: cell type diversification as an evolutionary strategy in angiosperm woods: fibre dimorphism in angiosperm wood. Bot. J. Linn. Soc. 174, 44–67. https://doi.org/10.1111/boj.12107.

Carvalho, A., Graça, C., Carocha, V., Pêra, S., Lousada, J.L., Lima-Brito, J., et al., 2015. An improved total RNA isolation from secondary tissues of woody species for coding and non-coding gene expression analyses. Wood Sci. Technol. 49, 647–658. https://doi.org/10.1007/s00226-015-0709-9.

Cavender-Bares, J., Cortes, P., Rambal, S., Joffre, R., Miles, B., Rocheteau, A., 2005. Summer and winter sensitivity of leaves and xylem to minimum freezing temperatures: a comparison of co-occurring Mediterranean oaks that differ in leaf lifespan. New Phytol. 168 (3), 597–612. https://doi.org/10.1111/j.1469-8137.2005.01555.x.

Chanoca, A., de Vries, L., Boerjan, W., 2019. Lignin engineering in forest trees. Front. Plant Sci. 10, 912. https://doi.org/10.3389/fpls.2019.00912.

Chitarra, W., Balestrini, R., Vitali, M., Pagliarani, C., Perrone, I., Schubert, A., et al., 2014. Gene expression in vessel-associated cells upon xylem embolism repair in Vitis vinifera L. Petioles. Planta 239, 887–899. https://doi.org/10.1007/s00425-013-2017-7.

Choat, B., Brodersen, C.R., McElrone, A.J., 2015. Synchrotron X-ray microtomography of xylem embolism in Sequoia sempervirens saplings during cycles of drought and recovery. New Phytol. 205, 1095–1105.

Colangelo, M., Camarero, J.J., Borghetti, M., Gentilesca, T., Oliva, J., Redondo, M.A., Ripullone, F., 2018. Drought and phytophthora are associated with the decline of oak species in southern Italy. Front. Plant Sci. 1595. https://doi.org/10.3389/fpls.2018.01595.

Corcuera, L., Camarero, J.J., Gil-Pelegrín, E., 2004. Effects of a severe drought on Quercus ilex radial growth and xylem anatomy. Trees 18, 83–92. https://doi.org/10.1007/s00468-003-0284-9.

Creek, D., Blackman, C.J., Brodribb, T.J., Choat, B., Tissue, D.T., 2018. Coordination between leaf, stem, and root hydraulics and gas exchange in three arid-zone angiosperms during severe drought and recovery. Plant Cell Environ. 41, 2869–2881. https://doi.org/10.1111/pce.13418.

David, T.S., Henriques, M.O., Kurz-Besson, C., Nunes, J., Valente, F., Vaz, M., et al., 2007. Water-use strategies in two co-occurring Mediterranean evergreen oaks: surviving the summer drought. Tree Physiol. 27 (6), 793–803. https://doi.org/10.1093/treephys/27.6.793.

De Micco, V., Aronne, G., Baas, P., 2008. Wood anatomy and hydraulic architecture of stems and twigs of some Mediterranean trees and shrubs along a Mesic-xeric gradient. Trees 22, 643–655. https://doi.org/10.1007/s00468-008-0222-y.

Encinas-Valero, M., Esteban, R., Hereş, A.-M., Becerril, J.M., García-Plazaola, J.I., Artexe, U., et al., 2021. Photoprotective compounds as early markers to predict holm oak crown defoliation in declining Mediterranean savannahs. Tree Physiol. 42, 208–224. https://doi.org/10.1093/treephys/tpab006.

Fan, Z.X., Zhang, S.B., Hao, G.Y., Ferry Slik, J.W., Cao, K.F., 2012. Hydraulic conductivity traits predict growth rates and adult stature of 40 asian tropical tree species better than wood density. J. Ecol. 100 (3), 732–741. https://doi.org/10.1111/j.1365-2745.2011.01939.x.

Feder, N., O'Brien, T.P., 1968. Plant microtechnique: some principles and new methods. Am. J. Bot. 55, 123–139.

Feltrim, D., Pereira, L., Costa, M.G.de S., Balbuena, T.S., Mazzafera, P., 2021. Stem aquaporins and surfactant-related genes are differentially expressed in two Eucalyptus species in response to water stress. Plant Stress 1, 100003. https://doi.org/10.1016/j.stress.2021.100003.

Flexas, J., Medrano, H., 2002. Drought-inhibition of photosynthesis in C3 plants: stomatal and non-stomatal limitations revisited. Ann. Bot. 89 (2), 183–189. https://doi.org/10.1093/aob/mcf027.

Flexas, J., Scoffoni, C., Gago, J., Sack, L., 2013. Leaf mesophyll conductance and leaf hydraulic conductance: an introduction to their measurement and coordination. J. Exp. Bot. 64, 3965–3981. https://doi.org/10.1093/jxb/ert319.

Fonti, P., Heller, O., Cherubini, P., Rigling, A., Arend, M., 2013. Wood anatomical responses of oak saplings exposed to air warming and soil drought. Plant Biol. 15, 210–219. https://doi.org/10.1111/j.1438-8677.2012.00599.x.

Fulton, D.C., Stettler, M., Mettler, T., Vaughan, C.K., Li, J., Francisco, P., et al., 2008. β-AMYLASE4, a noncatalytic protein required for starch breakdown, acts upstream of three active β-amylases in arabidopsis chloroplasts. Plant Cell 20, 1040–1058. https://doi.org/10.1105/tpc.107.056507.

Galiano, L., Martinez-Vilalta, J., Sabate, S., Lloret, F., 2012. Determinants of drought effects on crown condition and their relationship with depletion of carbon reserves in a Mediterranean holm oak forest. Tree Physiol. 32, 478–489. https://doi.org/10.1093/treephys/tps025.

Gärtner, H., Cherubini, P., Fonti, P., von Arx, G., Schneider, L., Nievergelt, D., et al., 2015. A technical perspective in modern tree-ring research - how to overcome dendroecological and wood anatomical challenges. JoVE, 1–10 https://doi.org/10.3791/52337.

Gentilesca, T., Camarero, J., Colangelo, M., Nolè, A., Ripullone, F., 2017. Drought-induced oak decline in the western Mediterranean region: an overview on current evidences, mechanisms and management options to improve forest resilience. iForest 10, 796–806. https://doi.org/10.3832/ifor2317-010.

Ghislain, B., Clair, B., 2017. Diversity in the organisation and lignification of tension wood fibre walls–A review. IAWA J. 38 (2), 245–265. https://doi.org/10.1163/22941932-20170170.

González-Rodríguez, V., Navarro-Cerrillo, R.M., Villar, R., 2011. Artificial regeneration with Quercus ilex L. And Quercus suber L. By direct seeding and planting in southern Spain. Ann. For. Sci. 68, 637–646. https://doi.org/10.1007/s13595-011-0057-3.

Gucci, R., Lombardini, L., Tattini, M., 1997. Analysis of leaf water relations in leaves of two olive (Olea europaea) cultivars differing in tolerance to salinity. Tree Physiol. 17, 13–21. https://doi.org/10.1093/treephys/17.1.13.

Hinckley, T.M., Duhme, A.R., Hinckley, A.R., Richter, H., 1980. Water relations of drought hardy shrubs: osmotic potential and stomatal reactivity. Plant Cell Environ. 3, 131–140. https://doi.org/10.1111/1365-3040.ep11580919.

Holbrook, N.M., 2002. The dynamics of "Dead Wood": maintenance of water transport through plant stems. Integr. Comp. Biol. 42, 492–496. https://doi.org/10.1093/icb/42.3.492.

Jensen, W.A., 1962. Botanical Histochemistry: Principles and Practice.

Jin, K.-M., Zhuo, R.-Y., Xu, D., Wang, Y.-J., Fan, H.-J., Huang, B.-Y., et al., 2020. Genome-wide identification of the expansin gene family and its potential association with drought stress in moso bamboo. IJMS 21, 9491. https://doi.org/10.3390/ijms21249491.

Joffre, R., Rambal, S., Ratte, J.P., 1999. The dehesa system of southern Spain and Portugal as a natural ecosystem mimic. Agrofor. Syst. 45, 57–79. https://doi.org/10.1023/A:1006259402496.

Johansen, D.A., 1940. Plant Microtechnique. 1st ed. McGraw-Hill, New-York.

Jupa, R., Plavcová, L., Gloser, V., Jansen, S., 2016. Linking xylem water storage with anatomical parameters in five temperate tree species. Tree Physiol. 36, 756–769. https://doi.org/10.1093/treephys/tpw020.

Kim, M.J., Kim, H., Shin, J.S., Chung, C.-H., Ohlrogge, J.B., Suh, M.C., 2006. Seed-specific expression of sesame microsomal oleic acid desaturase is controlled by combinatorial properties between negative cis-regulatory elements in the SeFAD2 promoter and enhancers in the 5′-UTR intron. Mol. Gen. Genomics. 276, 351–368. https://doi.org/10.1007/s00438-006-0148-2.

Kiorapostolou, N., Da Sois, L., Petruzzellis, F., Savi, T., Trifilò, P., Nardini, A., et al., 2019. Vulnerability to xylem embolism correlates to wood parenchyma fraction in angiosperms but not in gymnosperms. Tree Physiol. 39, 1675–1684. https://doi.org/10.1093/treephys/tpz068.

Kotrade, P., Sehr, E.M., Brüggemann, W., 2019. Expression profiles of 12 drought responsive genes in two european (deciduous) oak species during a two-year drought experiment with consecutive drought periods. Plant Gene 19, 100193. https://doi.org/10.1016/j.plgene.2019.100193.

Kubiske, M.E., Abrams, M.D., 1990. Pressure-volume relationships in non-rehydrated tissue at various water deficits. Plant Cell Environ. 13 (9), 995–1000. https://doi.org/10.1111/j.1365-3040.1990.tb01992.x.

Landhäusser, S.M., Chow, P.S., Dickman, L.T., Furze, M.E., Kuhlman, I., Schmid, S., et al., 2018. Standardized protocols and procedures can precisely and accurately quantify non-structural carbohydrates. Tree Physiol. 38, 1764–1778. https://doi.org/10.1093/treephys/tpy118.

Le Gall, H., Philippe, F., Domon, J.M., Gillet, F., Pelloux, J., Rayon, C., 2015. Cell wall metabolism in response to abiotic stress. Plants 4, 112–166. https://doi.org/10.3390/plants4010112.

Lens, F., Gleason, S.M., Bortolami, G., Brodersen, C., Delzon, S., Jansen, S., 2022. Functional xylem characteristics associated with drought-induced embolism in angiosperms. New Phytol. 236, 2019–2036. https://doi.org/10.1111/nph.18447.

Limousin, J.M., Roussel, A., Rodríguez-Calcerrada, J., Torres-Ruiz, J.M., Moreno, M., Garcia de Jalon, L., et al., 2022. Drought acclimation of Quercus ilex leaves improves tolerance to moderate drought but not resistance to severe water stress. Plant Cell Environ. 45 (7), 1967–1984. https://doi.org/10.1111/pce.14326.

Livak, K.J., Schmittgen, T.D., 2001. Analysis of relative gene expression data using real-time quantitative PCR and the $2-\Delta\Delta CT$ method. Methods 25, 402–408. https://doi.org/10.1006/meth.2001.1262.

Lopez, F., Bousser, A., Sissoëff, I., Gaspar, M., Lachaise, B., Hoarau, J., Mahé, A., 2003. Diurnal regulation of water transport and aquaporin gene expression in maize roots: contribution of PIP2 proteins. Plant Cell Physiol. 44 (12), 1384–1395.

Lopez, D., Venisse, J.-S., Fumanal, B., Chaumont, F., Guillot, E., Daniels, M.J., et al., 2013. Aquaporins and leaf hydraulics: poplar sheds new light. Plant Cell Physiol. 54, 1963–1975. https://doi.org/10.1093/pcp/pct135.

Lu, N., Ma, W., Han, D., Liu, Y., Wang, Z., Wang, N., et al., 2019. Genome-wide analysis of the Catalpa bungei caffeic acid O-methyltransferase (COMT) gene family: identification and expression profiles in normal, tension, and opposite wood. PeerJ 7, e6520. https://doi.org/10.7717/peerj.6520.

Madritsch, S., Wischnitzki, E., Kotrade, P., Ashoub, A., Burg, A., Fluch, S., et al., 2019. Elucidating drought stress tolerance in european oaks through cross-species transcriptomics. G3 Genes|Genomes|Genetics 9, 3181–3199. https://doi.org/10.1534/g3.119.400456.

Martin-StPaul, N., Delzon, S., Cochard, H., 2017. Plant resistance to drought depends on timely stomatal closure. Ecol. Lett. 20, 1437–1447. https://doi.org/10.1111/ele.12851.

McDowell, N.G., Ball, M., Bond-Lamberty, B., Kirwan, M.L., Krauss, K.W., Megonigal, J.P., Bailey, V., 2022. Processes and mechanisms of coastal woody-plant mortality. Glob. Chang. Biol. 28 (20), 5881–5900. https://doi.org/10.1111/gcb.16297.

Mertz, R.A., Brutnell, T.P., 2014. Bundle sheath suberization in grass leaves: multiple barriers to characterization. J. Exp. Bot. 65, 3371–3380. https://doi.org/10.1093/jxb/eru108.

Mittermeier, R.A., Turner, W.R., Larsen, F.W., Brooks, T.M., Gascon, C., 2011. Global biodiversity conservation: the critical role of hotspots. In: Zachos, F.E., Habel, J.C. (Eds.), Biodiversity Hotspots. Springer, Heidelberg, pp. 3–22.

Monroe, J.D., Storm, A.R., 2018. The arabidopsis β-amylase (BAM) gene family: diversity of form and function. Plant Sci. 276, 163–170. https://doi.org/10.1016/j.plantsci.2018.08.016.

Nagels Durand, A., Pauwels, L., Goossens, A., 2016. The ubiquitin system and jasmonate signaling. Plants 5, 6. https://doi.org/10.3390/plants5010006.

Nardini, A., Gullo, M.A.L., Trifilò, P., Salleo, S., 2014. The challenge of the Mediterranean climate to plant hydraulics: responses and adaptations. Environ. Exp. Bot. 103, 68–79. https://doi.org/10.1016/j.envexpbot.2013.09.018.

Noronha, H., Silva, A., Dai, Z., Gallusci, P., Rombolà, A.D., Delrot, S., et al., 2018. A molecular perspective on starch metabolism in woody tissues. Planta 248, 559–568. https://doi.org/10.1007/s00425-018-2954-2.

Ogaya, R., Barbeta, A., Başnou, C., Peñuelas, J., 2015. Satellite data as indicators of tree biomass growth and forest dieback in a Mediterranean holm oak forest. Ann. For. Sci. 72, 135–144. https://doi.org/10.1007/s13595-014-0408-y.

Ogaya, R., Liu, D., Barbeta, A., Peñuelas, J., 2020. Stem mortality and forest dieback in a 20-years experimental drought in a Mediterranean holm oak Forest. Front. For. Glob. Chang. 2, 89. https://doi.org/10.3389/ffgc.2019.00089.

Ohtsuka, A., Sack, L., Taneda, H., 2018. Bundle sheath lignification mediates the linkage of leaf hydraulics and venation. Plant Cell Environ. 41, 342–353. https://doi.org/10.1111/pce.13087.

Pagliarani, C., Casolo, V., Beiragi, M.A., Cavalletto, S., Siciliano, I., Schubert, A., et al., 2019. Priming xylem for stress recovery depends on coordinated activity of sugar metabolic pathways and changes in xylem sap pH. Plant Cell Environ. 42, 1775–1787. https://doi.org/10.1111/pce.13533.

Pasquini, D., Gori, A., Pollastrini, M., Alderotti, F., Centritto, M., Ferrini, F., Brunetti, C., 2023. Effects of drought-induced holm oak dieback on BVOCs emissions in a Mediterranean forest. Sci. Total Environ. 857, 159635. https://doi.org/10.1016/j.scitotenv.2022.159635.

Payyavula, R.S., Tay, K.H.C., Tsai, C.-J., Harding, S.A., 2011. The sucrose transporter family in populus: the importance of a tonoplast PtaSUT4 to biomass and carbon partitioning: tonoplast-localized sucrose transporter in populus. Plant J. 65, 757–770. https://doi.org/10.1111/j.1365-313X.2010.04463.x.

Peguero-Pina, J.J., Sancho-Knapik, D., Morales, F., Flexas, J., Gil-Pelegrín, E., 2009. Differential photosynthetic performance and photoprotection mechanisms of three Mediterranean evergreen oaks under severe drought stress. Funct. Plant Biol. 36 (5), 453–462. https://doi.org/10.1071/FP08297.

Peguero-Pina, J.J., Sancho-Knapik, D., Barrón, E., Camarero, J.J., Vilagrosa, A., Gil-Pelegrín, E., 2014. Morphological and physiological divergences within Quercus ilex support the existence of different ecotypes depending on climatic dryness. Ann. Bot. 114, 301–313. https://doi.org/10.1093/aob/mcu108.

Peguero-Pina, J.J., Sancho-Knapik, D., Martín, P., Saz, M.Á., Gea-Izquierdo, G., Cañellas, I., Gil-Pelegrín, E., 2015. Evidence of vulnerability segmentation in a deciduous Mediterranean oak (Quercus subpyrenaica EH del Villar). Trees 29, 1917–1927. https://doi.org/10.1007/s00468-015-1273-5.

Peguero-Pina, J.J., Mendoza-Herrer, Ó., Gil-Pelegrín, E., Sancho-Knapik, D., 2018. Cavitation limits the recovery of gas exchange after severe drought stress in holm oak (Quercus ilex L.). Forests 9 (8), 443. https://doi.org/10.3390/f9080443.

Perrone, I., Pagliarani, C., Lovisolo, C., Chitarra, W., Roman, F., Schubert, A., 2012. Recovery from water stress affects grape leaf petiole transcriptome. Planta 235, 1383–1396. https://doi.org/10.1007/s00425-011-1581-y.

Pfautsch, S., Renard, J., Tjoelker, M.G., Salih, A., 2015. Phloem as capacitor: radial transfer of water into xylem of tree stems occurs via symplastic transport in ray parenchyma. Plant Physiol. 167, 963–971. https://doi.org/10.1104/pp.114.254581.

Piva, T.C., Machado, S.R., Scremin-Dias, E., 2019. Anatomical and ultrastructural studies on gelatinous fibers in the organs of non-woody xerophytic and hydrophytic species. Botany 97, 529–536. https://doi.org/10.1139/cjb-2018-0220.

Piva, T.C., Fortuna-Perez, A.P., de Vargas, W., Machado, S.R., 2020. Variations in the architecture and histochemistry of the gelatinous fibers in eriosema (DC.) desv. (Leguminosae) species from the brazilian cerrado. Flora 268, 151624. https://doi.org/10.1016/j.flora.2020.151624.

Plavcová, L., Hacke, U.G., Almeida-Rodriguez, A.M., Li, E., Douglas, C.J., 2013. Gene expression patterns underlying changes in xylem structure and function in response to increased nitrogen availability in hybrid poplar: effects of nitrogen availability on xylogenesis. Plant Cell Environ. 36, 186–199. https://doi.org/10.1111/j.1365-3040.2012.02566.x.

Poorter, L., McDonald, I., Alarcón, A., Fichtler, E., Licona, J., Peña-Claros, M., et al., 2010. The importance of wood traits and hydraulic conductance for the performance and life history strategies of 42 rainforest tree species. New Phytol. 185, 481–492. https://doi.org/10.1111/j.1469-8137.2009.03092.x.

Rehschuh, R., Cecilia, A., Zuber, M., Faragó, T., Baumbach, T., Hartmann, H., Jansen, S., Mayer, S., Ruehr, N., 2020. Drought induced xylem embolism limits the recovery of leaf gas exchange in scots pine. Plant Physiol. 184 (2), 852–864. https://doi.org/10.1104/pp.20.00407.

Resco de Dios, V., Gessler, A., 2021. Sink and source co-limitation in the response of stored non-structural carbohydrates to an intense but short drought. Trees 35, 1751–1754. https://doi.org/10.1007/s00468-021-02116-9.

Resco de Dios, V., Arteaga, C., Peguero-Pina, J.J., Sancho-Knapik, D., Qin, H., Zveushe, O.K., et al., 2020. Hydraulic and photosynthetic limitations prevail over root non-structural carbohydrate reserves as drivers of resprouting in two Mediterranean oaks. Plant Cell Environ. 43, 1944–1957. https://doi.org/10.1111/pce.13781.

Rodríguez-Calcerrada, J., Li, M., López, R., Cano, F.J., Oleksyn, J., Atkin, O.K., et al., 2017. Drought-induced shoot dieback starts with massive root xylem embolism and variable depletion of nonstructural carbohydrates in seedlings of two tree species. New Phytol. 213 (2), 597–610. https://doi.org/10.1111/nph.14150.

Rodríguez-Calcerrada, J., Rodrigues, A.M., António, C., Perdiguero, P., Pita, P., Collada, C., et al., 2021. Stem metabolism under drought stress–a paradox of increasing respiratory substrates and decreasing respiratory rates. Physiol. Plant. 172 (2), 391–404. https://doi.org/10.1111/ppl.13145.

Saito, T., Soga, K., Hoson, T., Terashima, I., 2006. The bulk elastic modulus and the reversible properties of cell walls in developing quercus leaves. Plant Cell Physiol. 47 (6), 715–725. https://doi.org/10.1093/pcp/pcj042.

Salleo, S., Nardini, A., Lo Gullo, M.A., 1997. Is sclerophylly of Mediterranean evergreens an adaptation to drought? New Phytol 135, 603–612. https://doi.org/10.1046/j.1469-8137.1997.00696.x.

Sapes, G., Demaree, P., Lekberg, Y., Sala, A., 2021. Plant carbohydrate depletion impairs water relations and spreads via ectomycorrhizal networks. New Phytol. 229, 3172–3183. https://doi.org/10.1111/nph.17134.

Secchi, F., Zwieniecki, M.A., 2016. Accumulation of sugars in the xylem apoplast observed under water stress conditions is controlled by xylem pH. Plant Cell Environ. 39, 2350–2360. https://doi.org/10.1111/pce.12767.

Secchi, F., Pagliarani, C., Zwieniecki, M.A., 2017. The functional role of xylem parenchyma cells and aquaporins during recovery from severe water stress: response of xylem parenchyma cells to embolism. Plant Cell Environ. 40, 858–871. https://doi.org/10.1111/pce.12831.

Shatil-Cohen, A., Attia, Z., Moshelion, M., 2011. Bundle-sheath cell regulation of xylem-mesophyll watertransport via aquaporins under drought stress: a targetof xylem-borne ABA? Plant J. 67, 72–80. https://doi.org/10.1111/j.1365-313X.2011.04576.x.

Skelton, R.P., Dawson, T.E., Thompson, S.E., Shen, Y., Weitz, A.P., Ackerly, D., 2018. Low vulnerability to xylem embolism in leaves and stems of north american oaks. Plant Physiol. 177, 1066–1077. https://doi.org/10.1104/pp.18.00103.

Słupianek, A., Dolzblasz, A., Sokołowska, K., 2021. Xylem Parenchyma—Role and relevance in wood functioning in trees. Plants 10, 1247. https://doi.org/10.3390/plants10061247.

Smith-Martin, C.M., Skelton, R.P., Johnson, K.M., Lucani, C., Brodribb, T.J., 2020. Lack of vulnerability segmentation among woody species in a diverse dry sclerophyll woodland community. Funct. Ecol. 34 (4), 777–787. https://doi.org/10.1111/1365-2435.13519.

Srivastava, S., Vishwakarma, R.K., Arafat, Y.A., Gupta, S.K., Khan, B.M., 2015. Abiotic stress induces change in cinnamoyl CoA reductase (CCR) protein abundance and lignin deposition in developing seedlings of Leucaena leucocephala. Physiol. Mol. Biol. Plants 21, 197–205. https://doi.org/10.1007/s12298-015-0289-z.

Steppe, K., Cochard, H., Lacointe, A., Améglio, T., 2012. Could rapid diameter changes be facilitated by a variable hydraulic conductance?: variable hydraulic conductance facilitates rapid diameter changes. Plant Cell Environ. 35, 150–157. https://doi.org/10.1111/j.1365-3040.2011.02424.x.

Tenhaken, R., 2015. Cell wall remodeling under abiotic stress. Front. Plant Sci. 5. https://doi.org/10.3389/fpls.2014.00771.
Thalmann, M., Santelia, D., 2017. Starch as a determinant of plant fitness under abiotic stress. New Phytol. 214, 943–951. https://doi.org/10.1111/nph.14491.
Tomasella, M., Casolo, V., Aichner, N., Petruzzellis, F., Savi, T., Trifilò, P., et al., 2019a. Non-structural carbohydrate and hydraulic dynamics during drought and recovery in Fraxinus ornus and Ostrya carpinifolia saplings. Plant Physiol. Biochem. 145, 1–9. https://doi.org/10.1016/j.plaphy.2019.10.024.
Tomasella, M., Petrussa, E., Petruzzellis, F., Nardini, A., Casolo, V., 2019b. The possible role of non-structural carbohydrates in the regulation of tree hydraulics. IJMS 21, 144. https://doi.org/10.3390/ijms21010144.
Torres-Ruiz, J.M., Jansen, S., Choat, B., McElrone, A.J., Cochard, H., Brodribb, T.J., et al., 2015. Direct X-ray microtomography observation confirms the induction of embolism upon xylem cutting under tension. Plant Physiol. 167, 40–43. https://doi.org/10.1104/pp.114.249706.
Turner, N.C., 1988. Measurement of plant water status by the pressure chamber technique. Irrig. Sci. 9, 289–308. https://doi.org/10.1007/BF00296704.
Tyree, M.T., Richter, H., 1982. Alternate methods of analysing water potential isotherms: some cautions and clarifications. II. Curvilinearity in water potential isotherms. Can. J. Bot. 60, 911–916. https://doi.org/10.1139/b82-117.
Tyree, M.T., Davis, S.D., Cochard, H., 1994. Biophysical perspectives of xylem evolution: is there a tradeoff of hydraulic efficiency for vulnerability to dysfunction? IAWA J. 15 (4), 335–360.
Vanholme, R., Demedts, B., Morreel, K., Ralph, J., Boerjan, W., 2010. Lignin biosynthesis and structure. Plant Physiol. 153, 895–905. https://doi.org/10.1104/pp.110.155119.
Vaz, M., Pereira, J.S., Gazarini, L.C., David, T.S., David, J.S., Rodrigues, A., et al., 2010. Drought-induced photosynthetic inhibition and autumn recovery in two Mediterranean oak species (Quercus ilex and Quercus suber). Tree Physiol. 30 (8), 946–956. https://doi.org/10.1093/treephys/tpq044.
Vilagrosa, A., Bellot, J., Vallejo, V.R., Gil-Pelegrín, E., 2003. Cavitation, stomatal conductance, and leaf dieback in seedlings of two co-occurring Mediterranean shrubs during an intense drought. J. Exp. Bot. 54 (390), 2015–2024. https://doi.org/10.1093/jxb/erg221.
Wang, R., Zhang, L., Zhang, S., Cai, J., Tyree, M.T., 2014. Water relations of Robinia pseudoacacia L.: do vessels cavitate and refill diurnally or are R -shaped curves invalid in robinia ? Plant Cell Environ. 37, 2667–2678. https://doi.org/10.1111/pce.12315.
Western, T.L., 2012. The sticky tale of seed coat mucilages: production, genetics, and role in seed germination and dispersal. Seed Sci. Res. 22, 1–25. https://doi.org/10.1017/S0960258511000249.
Wu, Y., Meeley, R.B., Cosgrove, D.J., 2001. Analysis and expression of the α-expansin and β-expansin gene families in maize. Plant Physiol. 126 (1), 222–232. https://doi.org/10.1104/pp.126.1.222.
Yuan, L.-B., Dai, Y.-S., Xie, L.-J., Yu, L.-J., Zhou, Y., Lai, Y.-X., et al., 2017. Jasmonate regulates plant responses to postsubmergence reoxygenation through transcriptional activation of antioxidant synthesis. Plant Physiol. 173, 1864–1880. https://doi.org/10.1104/pp.16.01803.
Zeeman, S.C., Kossmann, J., Smith, A.M., 2010. Starch: its metabolism, evolution, and biotechnological modification in plants. Annu. Rev. Plant Biol. 61, 209–234. https://doi.org/10.1146/annurev-arplant-042809-112301.
Zimmermann, M., 1983. Xylem Structure and the Ascent of Sap. Springer.
Zwieniecki, M.A., Holbrook, N.M., 2009. Confronting Maxwell's demon: biophysics of xylem embolism repair. Trends Plant Sci. 14, 530–534. https://doi.org/10.1016/j.tplants.2009.07.00.